

Molecular Mechanism of HCl Acid Ionization in Water: *Ab Initio* Potential Energy Surfaces and Monte Carlo Simulations

Koji Ando[†] and James T. Hynes*

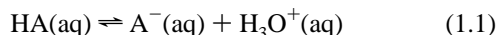
Department of Chemistry and Biochemistry, University of Colorado, Boulder, Colorado 80309-0125

Received: January 10, 1997[®]

The acid ionization of HCl in water is examined via a combination of electronic structure calculations with *ab initio* molecular orbital methods and Monte Carlo computer simulations. The following key features are taken into account in the modeling: the polarization of the electronic structure of the solute reaction system by the solvent, the quantum character of the proton nuclear motion, the solvent fluctuation and reorganization along with the solvent polarization effects on the proton potential, and a Grotthuss mechanism of the aqueous proton transfer. The mechanism is found to involve the following: first, a nearly activationless motion in a solvent coordinate, which is adiabatically followed by the quantum proton rather than tunneling, to produce a contact ion pair $\text{Cl}^- - \text{H}_3\text{O}^+$, which is stabilized by ~ 7 kcal/mol; second, motion in the solvent with a small activation barrier, as a second adiabatic proton transfer produces a solvent-separated ion pair from the contact ion pair in a nearly thermoneutral process. Motion of a neighboring water molecule—to accommodate the change of the primary coordination number from 4 for H_2O to 3 for H_3O^+ of a proton-accepting water molecule—is indicated as a key feature in the necessary solvent reorganizations. It is estimated, via a separate argument, that the remainder of the process to produce the completely separated ions involves a free energy change of less than 1 kcal/mol. It is argued that the reorganization of the heavy atoms between which the proton transfers plays an essential role in assisting the adiabatic (nontunneling) and stepwise transfer mechanism and that the concerted pathway of the multiple proton transfers in water is unfavorable.

I. Introduction

Proton transfer reactions represent a central elementary process in chemistry and biochemistry.^{1–5} In aqueous solution, the acid ionization



is of particular importance both *per se* and in connection with acid–base catalysis.^{3–5} But despite its prominence, the *molecular* mechanism of the solution phase reaction is unclear—thus, for example, it is not known if there is a barrier (or barriers) for eq 1.1 and in what coordinate it (or they) might exist. Beyond the complexity of the solution phase reaction, some reasons for this situation include (i) the alteration of the solute electronic structure, coupled to the solvation, in the reaction, (ii) the quantum nuclear character of the proton motion, and (iii) the specificity of proton transfers in water. In this work, we address these problems on the basis of a realistic molecular modeling—*ab initio* quantum chemistry calculations of the potential energy surfaces and Monte Carlo simulations—for HCl ionization in water.

Our treatment of this reaction is not a complete and entirely *ab initio* simulation, but rather involves an approach which is guided by and exploits earlier work on related systems in this laboratory.^{6–10} The basic perspective of our approach is as follows. First we note that the large polarity change in eq 1.1 indicates significant effects from the polar solvent, a well-appreciated feature for the overall reaction thermodynamics.⁴ Indeed, acid ionization does not occur in the isolated 1:1 hydrogen-bonded complex with H_2O ,¹¹ indicating that the ion

stabilization by the polar solvent water is essential for the reaction. Solvent fluctuation and reorganization are then expected to be critical factors in determining both the mechanism and the rate of the reaction. This aspect^{6–10,12} is similar to that for electron transfer reactions,¹³ excited electronic state charge-transfer state formations,¹⁴ and some unimolecular $\text{S}_{\text{N}}1$ ionizations¹⁵ in polar solvents, for which the free energy curve/surface crossing induced by the fluctuations of the polar environment is key. (The similarity is decidedly imperfect, since the quoted cases are characterized by weak electronic coupling between electrically diabatic states, whereas that coupling is strong for proton transfers.⁷ Nonetheless, the analogy is useful.) For the present proton transfer system, we postulate (and confirm within the present modeling) the following scheme, focusing for the moment and for simplicity solely on the first proton transfer between the HCl and a neighboring water molecule: the proton potential and its asymmetry are modulated by the fluctuating polar environment, and the proton transfer occurs at the “crossing” point of the solvent configuration which gives a symmetric proton potential (Figure 1). The asymmetry modulation of the proton potential can be qualitatively comprehended in terms of a valence-bond (VB) picture of the electronic structure;⁷ the relative stability between the neutral diabatic state ($\text{ClH} \cdots \text{OH}_2$) and the ionic one ($\text{Cl}^- \cdots \text{HOH}_2^+$), which varies with the solvent polarization fluctuation, alters the asymmetry of the (electronically) adiabatic proton potential curve. Since attainment of the crossing point by solvent motion will generally require thermal activation, the reaction coordinate is in this sense in the solvent, and there can be a free energy barrier in this coordinate. This behavior in the HCl case is in complete contrast to a view of the reaction in which the proton barrier height itself determines the activation energy for the rate.^{1,16,17} [This is not at all to say that the proton coordinate could not be usefully employed to analyze proton transfer reactions (see e.g.

[†] Present and permanent address: Institute of Materials Science, University of Tsukuba, Tsukuba, Ibaraki 305, Japan.

[®] Abstract published in *Advance ACS Abstracts*, April 15, 1997.

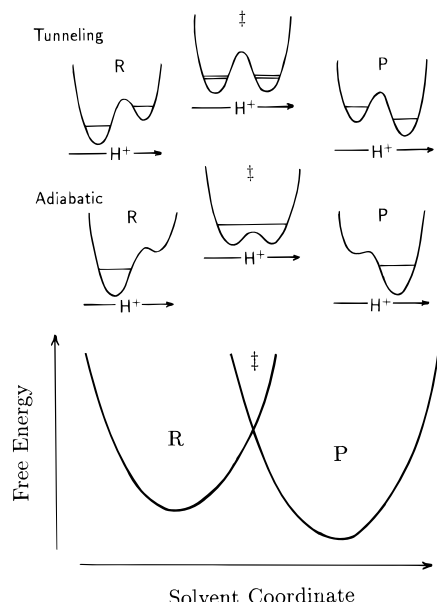


Figure 1. Schematic illustrations of (top and middle) the evolution of the proton transfer potential and (bottom) the two (diabatic) free energy curves in the solvent coordinate.

the path integral quantum Monte Carlo method in ref 18). Such a “quantum centroid” approach is also capable of capturing the solvent activation component of a rate constant.^{18c,d]}

The discussion above has been simplified for purposes of clarity. In particular, the crossing curves in the solvent coordinate of Figure 1 refer to solvent fluctuations in the respective presence of the two solute structures ($\text{ClH}\cdots\text{OH}_2$) and ($\text{Cl}^-\cdots\text{HOH}_2^+$). In reality, a more sophisticated description, as given within, is required in the neighborhood of the curve crossing. In addition, attention to the heavy atom separations Cl–O and O–O is required.

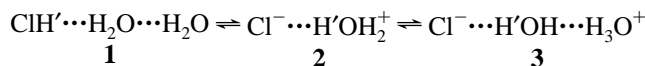
Second, we take account of the quantized nature of the proton nuclear motion, associated with the barrier height and shape of the proton potential. Depending on the strength of the hydrogen-bonding interaction, the height of the proton potential barrier and the position of the proton (vibrational) energy levels may vary in a way that controls the transfer mechanism. For “weak” hydrogen-bonding complexes where the barrier is high enough to hold several proton levels in either well, the proton transfer will be a quantum tunneling process.^{6,13b} In the case of “strong” hydrogen bonding, where the proton double well has a sufficiently low barrier such that the ground proton vibrational level, i.e. the zero-point energy, is located above the barrier top, the proton transfer is no longer tunneling, although it is still very much quantum in character (Figure 1). This key feature—which we will find applies to the HCl ionization—is in decided contrast to any classical, “over the proton barrier”, description^{1,16,17} of the reaction.

We call this last quantum situation an “adiabatic proton transfer”;^{8–10,18d–21} the proton wave packet motion adiabatically follows the modulation of the proton potential from the reactant solvent configuration through the diabatic crossing point to the product state (Figure 1). The distance between the heavy particles, between which the proton transfers, e.g. the oxygen atoms in an $\text{H}_3\text{O}^+\cdots\text{H}_2\text{O}$ arrangement, can be important in allowing this adiabatic pathway, since the proton barrier will be modulated by this separation.^{22,23}

Finally, we consider the role of the “Grotthuss mechanism”,^{4,5} which is quite specific for proton transfers in aqueous media: the solvent water molecules themselves can be involved in the process as proton acceptors. The first two proton transfer steps

may be illustrated as in Scheme 1. One remarkable aspect is

SCHEME 1



that a “proton relay” among water molecules may take place through the hydrogen-bonding network without the need of large displacements of an individual proton. This mechanism is believed to be the origin of the anomalously high mobility of the proton in water and ice^{4,22–26} and also is suggested to play an important role in various acid–base catalyses in aqueous solution, e.g. hydration–dehydration reactions, hydrolysis reactions, and other prototropic changes.^{3–5,27,28} A natural and interesting question then would be whether the double proton transfer is “stepwise” ($1 \rightarrow 2 \rightarrow 3$) or “concerted” ($1 \rightarrow 3$) in the case of HCl ionization.

The outline of this paper is as follows. After summarizing the quantum chemical and statistical mechanical computational methods in the next section—which regard the three molecule subsystem in Scheme 1 as the reacting solute system—we discuss the results of the solvent free energies and the proton potentials in section III for the first proton transfer step ($1 \rightarrow 2$) in Scheme 1, focusing on the above issues. Section IV is devoted to the second step ($2 \rightarrow 3$). This arrangement of the presentation anticipates that a stepwise route is favored compared to a concerted pathway; this specific issue is addressed in section V. In section VI, we discuss the expected impact on the present results of issues related to the solvent electronic polarization. The adiabaticity of the proton transfers is also discussed within the dynamic framework of a Landau–Zener curve-crossing model. A final section addresses the remainder of the ionization process in eq 1.1, as well as acid ionizations in related systems. A preliminary communication on this work has appeared.¹⁰

II. Potentials and Computational Methods

In this section, we describe the electronic structure and statistical mechanical methodology employed to examine the proton transfer sequence Scheme 1. Our basic orientation is to regard the trimer subsystem as the “solute” for the solution problem.

A. Electronic Structure Calculations. *Ab initio* molecular orbital (MO) methods²⁹ are used for three different purposes: (i) to optimize the nuclear geometries of small clusters, (ii) to determine the model potential functions used in subsequent Monte Carlo simulations, and (iii) to compute the potential energy surfaces as a function of proton coordinates. The restricted Hartree–Fock (RHF) and the second order Møller–Plesset (MP2) approximations³⁰ are employed with the 3-21G* (basis A) and 6-31G*(Cl+) (basis B) basis sets.³¹ The former set is used for geometry optimization, while the improved set is employed for determining various potentials. The standard 3-21G and 6-31G sets are augmented with d-polarization functions with the exponents of 0.8 and 0.75 on O and Cl atoms, respectively, and p-polarization functions with the exponent of 1.0 on H atoms are also supplied to the 6-31G set. In basis B, a set of p-type diffuse functions with the exponent of 0.049 is further placed on the Cl atom³² to better describe the diffuse anion Cl^- .

The MP2 approximation with this basis set quality (double- ζ plus polarization and diffuse) generally provides reliable ground electronic state energies in systems where the wave function is well represented by a Hartree–Fock configuration.^{30–33} This is expected to apply for the present cases, considering the small

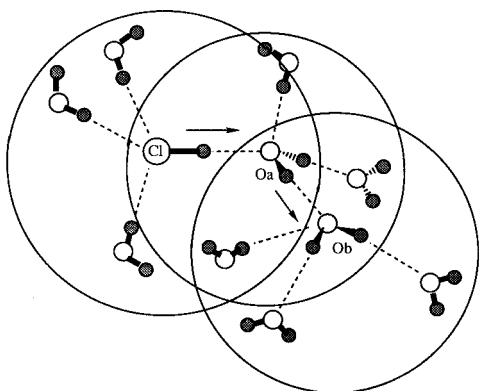


Figure 2. Schematic illustration of the primary reaction system $\text{ClH}\cdots\text{OH}_2\cdots\text{OH}_2$, with eight external waters displayed. See the text for explanation of the light line enclosures.

distance of the proton shifts (~ 0.6 Å) in the strongly overlapping hydrogen-bonded complexes. We have checked this aspect by carrying out calculations with the single and double-excitations configuration interaction (CI(SD)/3-21G**) method³⁴ for the proton shift, $\text{HCl}\cdots\text{H}_2\text{O} \rightarrow \text{Cl}^-\cdots\text{H}_3\text{O}^+$, with the equilibrium $\text{Cl}\cdots\text{O}$ distance (2.96 Å; see section II.B) at seven points of the proton displacement and found that the Hartree–Fock configuration dominates (the coefficient greater than 0.95) at every point.

With the use of the model potential functions developed in section II.C, Monte Carlo simulation (section II.D) for the solution phase reaction is carried out to construct free energy curves for the solvent coordinate.

B. Geometry Optimization of Small Clusters. As a preliminary to the full solution calculation, we first optimize the geometry of the reaction system **1** surrounded by eight water molecules, shown schematically in Figure 2. The eight external waters constitute the nearest-neighbor solvation around the reacting molecules **1**—each of whose three members (HCl , H_2O_a , and H_2O_b) is coordinated by four molecules. The analytic gradient method for the RHF wave function³⁵ is employed with basis A. Because of the practical difficulty in the full calculation of the whole system in Figure 2—due to the softness of the hydrogen-bonded complex compared to ordinary chemical bonds as well as to the large number of atoms—the geometries of small four-hydrated clusters designated by the thin curves in Figure 2 are optimized. First, the geometry of $\text{HCl}(\text{H}_2\text{O})_4$ is optimized in C_s symmetry. Second, the structure of H_2O_a surrounded by HCl and three waters is determined, where the HCl bond distance is fixed to the value obtained in the first optimization (see the last paragraph of this subsection). Finally, the four-hydration structure of H_2O_b is optimized. For $\text{H}_2\text{O}_a\cdots\text{HCl}(\text{H}_2\text{O})_3$ and $\text{H}_2\text{O}_b\cdots(\text{H}_2\text{O})_4$, no symmetry is assumed and all the hydrogen-bonds are constrained to be linear. The optimized heavy atom distances $\text{Cl}\cdots\text{O}_a$ and $\text{O}_a\cdots\text{O}_b$, and the $\text{Cl}-\text{H}$ (r_1) and O_a-H (r_2) bond lengths are 2.96, 2.83, 1.33, and 0.98 Å respectively.

A stable ion pair state corresponding to **2** is not found in the smaller $\text{HCl}(\text{H}_2\text{O})_4$ cluster, as it seems to require reorganization of at least six waters surrounding the pair (see also section VII). Instead of repeating the geometry optimizations for the ion pair states **2** and **3** (at possibly much higher computational costs), we have employed a simplified procedure as follows: we (i) shift the transferring proton(s) to the H_3O^+ site fixing the other atoms, (ii) determine model potential functions for the isolated trimers **2** and **3** as in section II.C below, (iii) reorganize eight external waters by using the model potentials, and (iv) compute the proton potentials with the resulting external configurations. (Related discussions are given in sections III.B and VII.)

We have also examined the structure change associated with an increase in the hydration number of HCl . By hydrating HCl successively, $\text{HCl}(\text{H}_2\text{O})_n$, $n = 0-4$, we find a reduction of the $\text{Cl}\cdots\text{O}_a$ heavy atom distance (3.085, 3.052, 3.055, and 2.928 Å for $n = 1-4$) and an extension of the $\text{Cl}-\text{H}$ bond length (1.268, 1.287, 1.292, 1.295, and 1.325 Å for $n = 0-4$).³⁶ These features indicate an enhancement of the polarity of HCl due to hydration. In simplified VB language,⁷ this would be comprehended as a solvent polarization favoring the ion pair component of the wave function compared to a neutral pair component.

C. Model Potential Functions. It is impractical to carry out quantum chemical calculations corresponding to those in section II.B above including hundreds of water molecules necessary for the solution calculations. For this purpose then, we describe a procedure by which the many water molecules external to the basic reaction system **1-3** are accounted for via model potential energy functions, using information from the electronic structure calculations of section II.B.

We determine model potential parameters to be used in the Monte Carlo simulations in the potential form

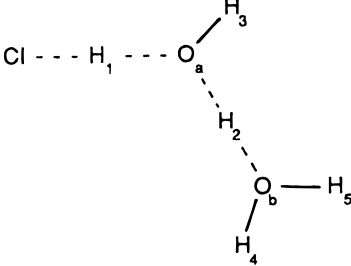
$$V_{\text{int}} = \sum_a \sum_b \left[\frac{q_a q_b}{r_{ab}} + 4\epsilon_{ab} \left\{ \left(\frac{\sigma_{ab}}{r_{ab}} \right)^{12} - \left(\frac{\sigma_{ab}}{r_{ab}} \right)^6 \right\} \right] \quad (2.1)$$

The electrostatic term here represents the Coulomb interaction between point charges on each atomic site. The point charges on the external waters are taken from the TIP3P model for water.³⁷ The point charges on the reaction system **1-3** are determined so as to reproduce the electrostatic potentials at ~ 500 points (from the van der Waals surface of the trimer to a distance of 27 Å—sufficient to attain convergence) around the trimers **1-3** computed from the electron density matrix of the RHF wave function with basis B. To include the solvent-induced polarization of the solute, RHF (basis B) wave functions of the system **1-3** are recalculated under the influence of eight external waters reorganized to each charge distribution of the systems **1-3** (cf. sections II.B and III.B). For the ion pair states **2** and **3**, the cluster structures optimized by using the model potential eq 2.1 with the charge distribution of the isolated **2** and **3** structures are used. The resultant point charge parameters are listed in Table 1. The charges for the isolated systems **1-3** are also included in the table for comparison with these, which clearly indicate the solvent-induced polarization of the system. It is also worth pointing out that there is a certain charge delocalization throughout the system. For example, the net charge in Cl in structures **2** and **3** is -0.846 and -0.910 , respectively, rather than a unit negative charge.

The LJ parameters ϵ and σ in eq 2.1 are determined so as to approximate the interaction energies and the average heavy atom ($\text{Cl}\cdots\text{O}$ and $\text{O}\cdots\text{O}$) distances for the smaller clusters $\text{HCl}(\text{H}_2\text{O})_4$, $\text{Cl}^-(\text{H}_2\text{O})_4$, and $\text{H}_3\text{O}^+(\text{H}_2\text{O})_3$. The reference energies and geometries to be approximated are taken from MP2 energy calculations with basis B and RHF geometry optimizations with basis A, respectively. The determined parameters as well as the reference quantities in the procedure are summarized in Table 2. Checks on these potentials are described in section II.E.

D. Monte Carlo Simulations. To determine the free energies in the solvent coordinate (to be defined subsequently) for the full solution calculations, Monte Carlo simulations are carried out using standard procedures³⁸ with Metropolis sampling, periodic boundary conditions, and the canonical (constant NVT) ensemble. Each cubic cell contains the reaction system **1, 2, or 3** and 248 water molecules. The temperature is fixed at 298 K. The box length is 19.6 Å, so that the mass density

TABLE 1: Point Charge Parameters



O–O Distance = 2.83 Å						
	1		2		3	
Cl	0.417	(−0.348) ^a	−0.846	(−0.770)	−0.910	(−0.857)
H ₁	0.298	(0.212)	0.327	(0.284)	0.411	(0.352)
O _a	−0.975	(−0.744)	−0.593	(−0.529)	−0.931	(−0.755)
H ₂	−0.542	(0.420)	0.543	(0.481)	0.417	(0.403)
H ₃	0.542	(0.420)	0.543	(0.481)	0.534	(0.421)
O _b	−0.970	(−0.802)	−0.980	(−0.813)	−0.565	(−0.536)
H ₄	0.490	(0.421)	0.503	(0.433)	0.522	(0.496)
H ₅	0.490	(0.421)	0.503	(0.433)	0.522	(0.496)

O–O Distance = 2.56 Å						
	1		2		3	
Cl	−0.396	(−0.355)	−0.853	(−0.776)	−0.895	(−0.844)
H ₁	0.260	(0.216)	0.342	(0.290)	0.379	(0.340)
O _a	−0.928	(−0.763)	−0.643	(−0.552)	−0.890	(−0.761)
H ₂	0.508	(0.418)	0.550	(0.480)	0.463	(0.424)
H ₃	0.508	(0.418)	0.550	(0.480)	0.517	(0.431)
O _b	−0.956	(−0.786)	−0.960	(−0.800)	−0.632	(−0.570)
H ₄	0.502	(0.426)	0.507	(0.439)	0.529	(0.490)
H ₅	0.502	(0.426)	0.507	(0.439)	0.529	(0.490)

^a Values in parentheses are those determined for the isolated trimers 1–3.

TABLE 2: Lennard-Jones Parameters

	HCl	Cl [−]	H ₃ O ⁺
<i>n</i>	4 ^a	4	3
\bar{R}_{OX}^d (ref) ^b	3.62	3.37	2.58
R_{OX} (model)	3.43	3.37	2.58
V_{int}^e (ref) ^c	−17.3	−49.8	−90.2
V_{int} (model)	−17.3	−50.1	−90.3
σ_{OX}^d	3.41	3.63	2.63
ϵ_{OX}	1.13	0.369	2.44

^a A cluster with the hydration number $n = 4$ is considered, while the fitting procedure is carried out for the three waters other than the proton-accepting water. ^b Average aqueous oxygen–X atoms distance (X = Cl or O) in the hydration clusters computed from the 3-21G*/RHF geometry optimizations. ^c MP2 hydration energies calculated with the 6-31G** (Cl[−]) basis set (basis B) for HCl, Cl[−], or H₃O⁺ and the 6-31G* set for water. ^d \bar{R}_{OX} and σ_{OX} are given in Å. ^e V_{int} and ϵ_{OX} are given in kcal/mol.

of the system is 0.997 g/cm³. New configurations are generated by randomly selecting a solvent molecule, translating its center-of-mass in three space-fixed Cartesian directions by randomly determined distances, and rotating it by displacing the three Euler angles by randomly determined amounts. The ranges of the translational and angular displacements are ± 0.15 Å and $\pm 5^\circ$, respectively. For one of the three Euler angles, its cosine is displaced within a range of $\pm 5/180$, in order to avoid the singularity associated with the use of Euler angles.³⁸ The ranges chosen here yield the acceptance ratios of 0.4–0.5 for new configurations. Each simulation starts with an equilibration run with more than 5×10^5 configuration generations. Additional runs are carried out to compute the free energy curves, which consist of several (4–8) sets of 1×10^6 configuration genera-

tions. The intermolecular interactions are spherically truncated at a cutoff distance of half the box length, referenced to the center-of-mass distance of each molecule.

E. Potential Energy Checks. To further check the quality of the model potential functions determined by the procedures described in section II.C, the radial distribution functions (rdf's) are computed for the chloride anion isolated in water. The simulation method is basically the same as in section II.D. The number of the solvent water molecules around Cl[−] is 250. The modified Owicki method³⁹ is employed for an efficient configuration sampling around the anion. More than 4×10^6 configurations are generated for equilibration, and additional 5×10^6 configurations are used to compute the rdf's.

It was found that the ion–oxygen and the ion–hydrogen rdf's displays a first peak at the distance 3.3 and 2.5 Å, respectively, which are in reasonable agreement with the experimental data. (X-ray diffraction,⁴⁰ 3.10–3.35 Å for the ion–oxygen distance; neutron diffraction,⁴¹ 3.20–3.34 and 2.22–2.26 Å for ion–oxygen and ion–hydrogen distances.) The coordination numbers of Cl[−] defined by integration to the minimum after the first peak in the ion–oxygen and ion–hydrogen rdf's are computed to be 7.9 and 7.0. X-ray and neutron diffraction experiments give the coordination number of 5–11⁴⁰ and 5.3–6.2,⁴¹ respectively. Considering the octet structure for the valence electrons, four waters are expected to participate in the hydrogen bonding to Cl[−]; this is the basis of our choice of external waters in the cluster calculations described in section II.B and shown in Figure 2. As discussed in section VII, those eight external waters represent the essential features of the solvent reorganization effects on the proton potential. The hydration numbers obtained here are comparable to those of previous simulation results:^{42–46} 7.4 (7.0), 5.6, 8.36, 7.4, and 7.2. These larger numbers compared to the neutron diffraction data and to the octet structural consideration might be a consequence of the model potential form eq 2.1 employed.⁴⁷ However, as mentioned above (see also section VII), the small uncertainty in the hydration number does not seem critical for the present argument.

F. Free Energy Calculations. The solvent coordinate referred to in the Introduction and in section II.D is defined by the energy difference of the diabatic states

$$\Delta E_{ij} \equiv V_i(\mathbf{S}; \mathbf{R}_i) - V_j(\mathbf{S}; \mathbf{R}_j) = \Delta V_{ij}(\mathbf{S}) \quad (2.2)$$

where $V_i(\mathbf{S}; \mathbf{R}_i)$ denotes the total potential energy including the solute internal, solute–solvent interaction, and solvent–solvent interaction energies at a fixed solute coordinate \mathbf{R}_i , as a functions of the solvent configuration \mathbf{S} , i.e., ΔE gauges the relative energetics of two solute states at a given solvent configuration. The subscripts i, j denote the diabatic states corresponding to 1–3. Specifically, we will consider $(i, j) = (1, 2)$ and $(2, 3)$ which represent the first and the second proton transfer steps, respectively, and also $(1, 3)$ for the concerted pathway. At each solvent configuration in the Monte Carlo simulation, all the interaction energies for the three diabatic states, $V_i(\mathbf{S}; \mathbf{R}_i)$ $i = 1–3$, are computed by switching the proton coordinates (r_1, r_2) and the potential parameters, while the Metropolis test for the acceptance of new configurations refers to one of the energies or the linear combination of the two (see eq 2.6 below).

The free energy curves $G_i(\Delta E_{ij})$ are defined by

$$G_i(\Delta E_{ij}) = -k_B T \ln Q_i(\Delta E_{ij}) \quad (2.3)$$

where $Q_i(\Delta E_{ij})$ is the partition function given (apart from an irrelevant constant factor) by

$$Q_i(\Delta E_{ij}) = \int \delta(\Delta E_{ij} - \Delta V_{ij}(\mathbf{S})) \exp(-V_i(\mathbf{S}; \mathbf{R}_i)/k_B T) d\mathbf{S} \quad (2.4)$$

which is connected to the probability density by

$$P_i(\Delta E_{ij}) = \frac{Q_i(\Delta E_{ij})}{Z_i}; \quad Z_i = \int \exp(-V_i(\mathbf{S}; \mathbf{R}_i)/k_B T) d\mathbf{S} \quad (2.5)$$

$P_i(\Delta E_{ij})$ is directly computed by the simulation. In practice, eqs 2.3–2.5 with a finite Monte Carlo sampling give only a small region of the curve around the minimum of G , whereas high free energy regions near the diabatic crossings are also critical in elucidating the reaction mechanism. To access these regions, we apply the free energy perturbation method⁴⁸ with an intermediate potential

$$V_\alpha(\mathbf{S}) = V_i(\mathbf{S}; \mathbf{R}_i) + \alpha(V_j(\mathbf{S}; \mathbf{R}_j) - V_i(\mathbf{S}; \mathbf{R}_i)) \quad (2.6)$$

The interpolation of the free energy curves is realized by varying the parameter α from 0 to 1 using

$$G_\alpha(\Delta E) - G_{\alpha'}(\Delta E) = -k_B T \ln [P_\alpha(\Delta E)/P_{\alpha'}(\Delta E)] + C_{\alpha\alpha'}$$

$$C_{\alpha\alpha'} = -k_B T \ln \langle \exp(-(\alpha - \alpha')\Delta V_{\alpha\alpha'}(\mathbf{S})/k_B T) \rangle_\alpha \quad (2.7)$$

$$= +k_B T \ln \langle \exp(+(\alpha - \alpha')\Delta V_{\alpha\alpha'}(\mathbf{S})/k_B T) \rangle_{\alpha'}$$

The solvation effects from outside of the spherical truncation are estimated by the reaction field approximation,³⁸ $G_{\text{rf}} = (\epsilon - 1)/(2\epsilon + 1) \cdot \mu^2/(L/2)^3$, where ϵ , μ , and L are the static dielectric constant of water, the dipole moment of the solute **1**, **2**, or **3**, and the simulation box length, respectively. These values are computed (at the O–O distance 2.83 Å, see sections III and IV) to be $\Delta G_{23}^{\text{fld}} = 1.22$ kcal/mol where, for example, the subscript 12 means the difference between states **1** and **2** as in the solvent coordinate $\Delta E_{1/2}$ (cf. eq 2.2). The solution internal energy is expressed as a function of ΔE by interpolation with a form $V^{\text{solute}}(\Delta E) = a(\tanh(b(\Delta E - c)) + d)$. For example, the parameter a is typically 2–3 kcal/mol. The simulation uncertainty in the computed free energy curves is estimated to be ± 0.3 kcal/mol (see below for details).

III. First Proton Transfer Step

A. Potential Energy Surfaces. We first present the results for the first proton transfer **1** \rightarrow **2** in Scheme 1 within a stepwise assumption. The Cl–O and O–O distances are taken to be 2.96 and 2.83 Å, respectively, which are the distances obtained in section II.B appropriate for the neutral state **1**.

Figure 3 displays the free energy curves in the solvent coordinate ΔE_{12} . These curves are obtained by the Monte Carlo sampling together with a free energy perturbation method to access the thermally improbable regions of high free energy, as described in section II.F. Several points from around the edges of the sampling windows, i.e., the low-probability regions for each α value, were discarded, which still preserves data from different α values that are well overlapped. We stress here that by using eq 2.7, we need no artificial adjustment in order to connect data of different α values. The simulation uncertainty of the free energy was evaluated from its variance at given ΔE_{12} coordinates where three or more points are obtained from different α values. The average variance was computed to be 0.23 kcal/mol. [A similar analysis of the second proton transfer step (section IV) gives ≈ 0.26 kcal/mol.]

It is noted that the free energy curves computed from Monte Carlo sampling are well approximated by parabolas with the

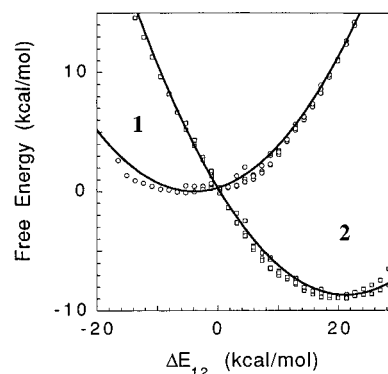


Figure 3. Diabatic free energy curves in the solvent coordinate ΔE_{12} . The circle and box marks are from the Monte Carlo sampling with $\alpha = 0.0, 0.2, 0.4, 0.6, 0.8, 0.9$, and 1.0 (see eq 2.7). The solid curves are the least-squares parabolic fit with the same force constants for both the reactant and product curves.

same force constant for both the reactant and the product curves.⁴⁹ The root-mean-square (rms) deviation of the numerical fitting is 0.80 kcal/mol.⁵⁰ The solvent reorganization energy for the first step **1** \rightarrow **2** is computed to be 12.6 kcal/mol. The rather large reorganization energy indicates that the equilibrium solvation states for the reactant **1** and the contact ion pair product **2** are well separated from each other in the solvent coordinate.

These calculations then provide the starting point for the determination of the proton potentials. In particular, solvent configurations corresponding nominally to the reactant ($\Delta E_{12} < 0$), the product ($\Delta E_{12} > 0$), and the intersection $\Delta E_{12} = 0$ in Figure 3 are then used as configurations for which to generate the potential for the proton transfer in the fixed field of the solvent molecules, as described in the next paragraph. The solvent configurations are sampled in the course of the Monte Carlo simulations. First, the equilibrium average values of the solute–solvent and the solvent–solvent interaction energies are computed for each of the solute states **1** and **2**. Additional Monte Carlo runs are continued until these energies coincide with the average values within ± 0.1 kcal/mol. We also sample the solvent configurations at the diabatic crossing point of the solvent free energy curves, which are expected to give a symmetric proton potential curve. For this purpose, 5×10^5 configurations are first generated with an additional parabolic umbrella potential of form $U(\Delta E_{12}) = a\Delta E_{12}^2$, with a equal to 1.0 (kcal/mol)^{−1}. The simulation is continued until the system comes to the diabatic crossing point $\Delta E_{12} = 0$ to within ± 0.1 kcal/mol.

The MP2 wave function with basis B (cf. section II.A) is employed to compute the proton potential energy surfaces. To be consistent with the spherical truncation of the interaction energy in the Monte Carlo simulation, the solvent molecules outside the sphere, i.e. around the simulation box edges, are discarded; this results in an inclusion of ~ 130 solvent waters. The point charges on each atomic site of the solvent waters are taken from the TIP3P model, as noted in section II.C. The inclusion of the point charge amounts to additional terms in the one-electron operator in the self-consistent field (SCF) equations at essentially no computational cost. The point charge approximation includes only the electrostatic component, but not the exchange-exclusion part (modeled by the LJ terms in eq 2.1), of the solute–solvent interaction. The latter would be reasonably constant in the course of the proton shift with the fixed heavy atoms configurations.

Figure 4 displaying the resulting proton potential curves confirms the postulated scheme of section I for the HCl proton transfer in water: the fluctuating polar environment modulates

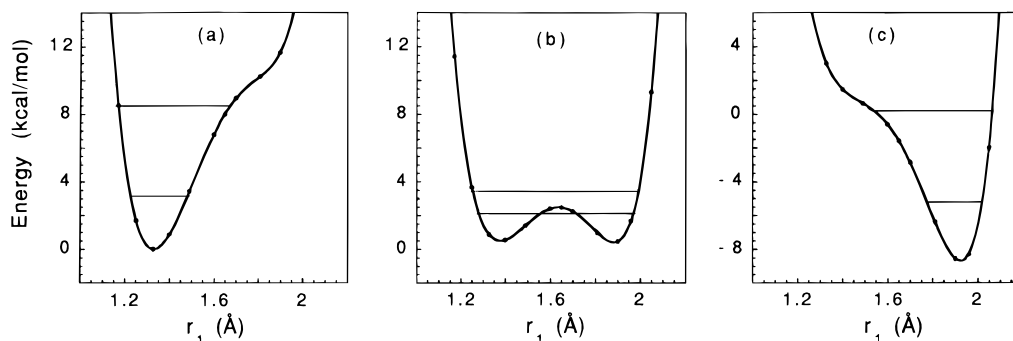


Figure 4. Proton transfer potentials evaluated at (a) $\Delta E_{12} < 0$, (b) $\Delta E_{12} = 0$, and (c) $\Delta E_{12} > 0$, with the ground (zero-point energy) and the first excited proton vibrational level displayed. The Cl–O distance is 2.96 Å. The dot marks are the computed points, and the curves are obtained by spline interpolation. The variance of the calculated proton barrier height in (b) for five different independent solvent configuration samplings (all with $\Delta E_{12} = 0$) is 0.1 kcal/mol. (The variance of the average of the forward and reverse barrier heights is ~ 0.01 kcal/mol).

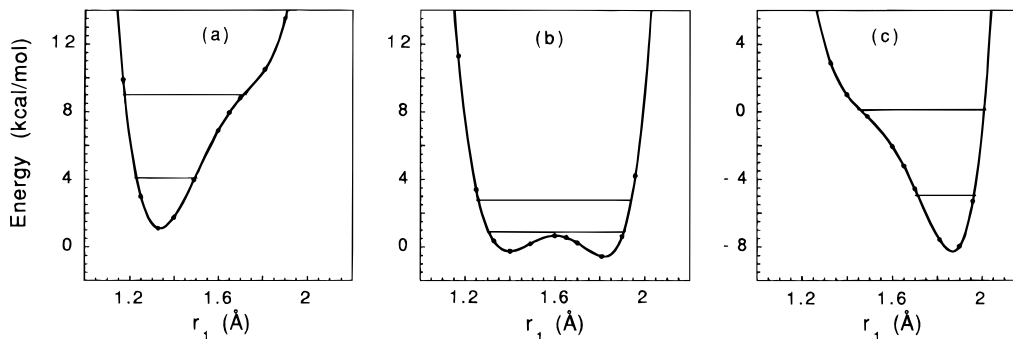


Figure 5. Same as Figure 4, but the Cl–O distance is 2.91 Å. The same solvent configurations as those in each of Figure 4a–c are used.

the proton potential asymmetry, and the proton transfer can occur at the “crossing” point of the solvent free energy curves. It is also seen in the figure that the proton potential at $\Delta E_{12} = 0$ is symmetric and that the calculated (from a one-dimensional Schrödinger equation numerically solved by a renormalized Numerov method⁵¹) ground adiabatic state proton vibrational level is slightly below the proton barrier top. In fact, as to be discussed in section VI, any simulation—such as the present one—which in effect treats the solvent electronic polarization classically and via effective charges on the solvent molecules, will give an *overestimate* of the proton barrier. Thus the true proton barrier will be lower than that displayed, and the proton vibrational level will be above it. This last feature signals an adiabatic proton transfer.

There is another issue concerning the adiabaticity. The proton barrier height is known to be very sensitive to the heavy atoms’s distance between which the proton transfers^{6,22,52} (in this case, the Cl–O distance). Ideally, the proton adiabaticity should be considered with the (quantum) distribution of the Cl–O distance. Further, we have seen in section II.B that the Cl–O distance decreases by increasing the hydration number in the cluster—arising from polarity enhancement due to hydration. In view of these aspects, we have examined a very small (0.05 Å) compression of the Cl–O distance—which is small enough to be within the quantum delocalization of the Cl–O zero-point vibrational wave function—and to be within a possible uncertainty of the Cl–O distance due to the hydration aspect above. The resultant proton potentials are displayed in Figure 5. It is seen that now the proton ground vibrational level is slightly above the barrier top at the diabatic crossing $\Delta E_{12} = 0$. Therefore both the solvent electronic polarization effect and the Cl–O vibrational fluctuation suggest that this proton transfer is indeed adiabatic.

Returning to the main thread, the entire discussion above has relied on the calculation of proton transfer potentials at given (different) ΔE_{12} values. But there are many solvent configura-

tions with the same given ΔE_{12} value, and one should ask if there are changes due to different solvent configuration samplings. The variance of the proton barrier height among different samplings is checked to be small (0.1 kcal/mol) for the symmetric curve shown in Figure 4b. The proton potential is indeed affected by these solvent configurational fluctuations at fixed ΔE_{12} . But since the variation of the proton potential due to sampling is small at fixed ΔE_{12} , the solvent polarization is well characterized by the ΔE_{12} coordinate, and in fact the proton asymmetry is directly connected to ΔE_{12} .

The picture for the first transfer $1 \rightarrow 2$ that emerges is then the following. The acid–base proton transfer is quantum adiabatic, rather than tunneling, with the proton adiabatically following the slow solvent rearrangement to configurations with $\Delta E_{12} = 0$. This rearrangement occurs at a slight cost of free energy.

The precise cost to reach the transition state in the solvent coordinate is calculated as follows. We determine the vibrational energy levels for the proton in the reactant and at the transition state in ΔE_{12} and at various other points, by solving the Schrödinger equation for the proton in its potential in those ΔE_{12} regions. The variation of the proton potential due to the solvent polarization fluctuation is described by interpolation in the ΔE_{12} coordinate. These final results, which also include the solvent self-free energy, are designated by the small cross marks in Figure 6. It is then seen that the process is nearly barrierless: $\Delta G_{12}^{\ddagger} = 0.1$ kcal/mol. In a similar way, a reaction free energy of $\Delta G_{12} = -6.7$ kcal/mol is estimated. Thus the adiabatic $1 \rightarrow 2$ transfer is an almost activationless process in the solvent coordinate and is markedly downhill in free energy. By contrast, we calculate $1 \rightarrow 2$ transfer to be uphill by ~ 20 kcal/mol in the isolated HCl–H₂O complex, where the Cl–O distance is 2.96 Å.

As described in the second paragraph of this section, the estimated error in ΔG_{12} is about ± 0.3 kcal/mol. The error in

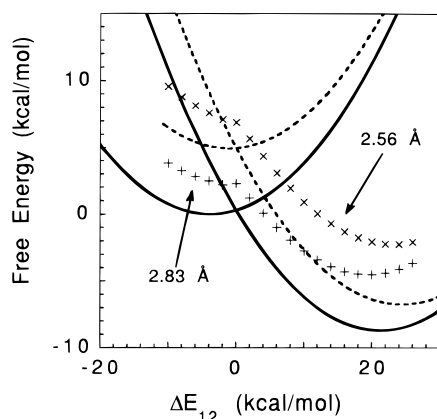


Figure 6. Diabatic free energy curves in the solvent coordinate ΔE_{12} , with the ground proton vibrational levels (including the solvent self-free energy) designated by (+++) and (xxx) marks. The O—O distance is (—, +++) 2.83 Å and (---, xxx) 2.56 Å. The solid curves are taken from Figure 3.

ΔG_{12}^{\ddagger} can be evaluated as follows: By using the Marcus relation $\Delta G^{\ddagger} = (\Delta G + \Delta G_r)^2 / 4\Delta G_r$, which we found above to be a reasonable approximation for our diabatic free energy curves in the ΔE_{12} coordinate, the error in ΔG^{\ddagger} is evaluated to be $\delta\Delta G^{\ddagger} = (\Delta G^{\ddagger}/\Delta G_r)^{1/2}\delta\Delta G$. Inserting the computed values of the diabatic curves, we obtain $\delta\Delta G^{\ddagger} \approx 0.07$ kcal/mol. We note, however, that this estimate relies on the approximation of the Marcus relation. The actual error is expected to be between this and the estimated error of the exothermicity $\delta\Delta G = 0.3$ kcal/mol.

The calculations above were performed at an O—O distance of 2.83 Å between the two explicit waters in Scheme 1. This is the equilibrium distance between two neutral water molecules in $(\text{H}_2\text{O})_5$. When the above calculations are repeated at an O—O distance value of 2.56 Å—the $\text{H}_3\text{O}^+ - \text{H}_2\text{O}$ equilibrium distance in $\text{H}_3\text{O}^+(\text{H}_2\text{O})_3$ —the same basic picture emerges for the proton potentials and the vibrational levels. However, the compression of the O—O distance costs free energy in the amount of 4.9 kcal/mol in the neutral state **1**—computed by the Monte Carlo simulation taking account of the total potential energy of the solution phase—and thus is strongly disfavored. The free energy curves as well as the final adiabatic ones considering the proton vibrational levels displaying these aspects are included in Figure 6.

We now consider for perspective a contrasting view of the reaction. It is seen from the definitions in eqs 2.2–2.5 that the one-dimensional curve $G_i(\Delta E_{ij})$ corresponds to a cut along a fixed r_i of a global two-dimensional free energy surface $G_i(\Delta E_{ij}, r_i)$. Figure 7 shows the surface $G(\Delta E_{12}, r_1)$ constructed by combining $G(\Delta E_{12})$ curves and the proton potential curves by interpolation. In contrast to the mechanism we have described above, the solid curve included in the figure follows the equilibrium solvation path, i.e., the free energies minimized in the ΔE_{12} coordinate at each fixed proton position r_1 —this assumes that the solvent motion is fast compared to the proton motion. Its profile along r_1 is a mean force (mf) potential for the proton. However, in our perspective, consideration of the free energy surface and the quantized character of the proton motion implies that the *dynamical mechanism* of the proton transfer naturally involves a nonequilibrium solvation situation in which the proton is fast compared to the solvent.^{7,53–55}

Finally, we observe that the reaction free energy of the **1** → **2** proton transfer is calculated to be −6.7 kcal/mol. The experimental overall reaction free energy for reaction eq 1.1 is estimated⁵⁶ to be −8 to −10 kcal/mol. Thus the major portion

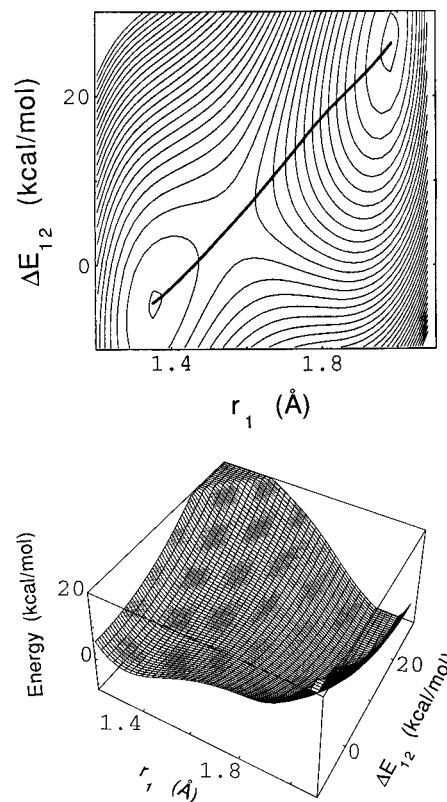


Figure 7. Two-dimensional free energy surface as a function of the proton coordinate r_1 and the solvent coordinate ΔE_{12} . The solid curve on the surface is the equilibrium solvation path. Contour spacing is 1 kcal/mol.

of the overall reaction free energy is calculated to occur in the very first step.

B. Small Clusters and Nearest-Neighbor Solvation. What solvent rearrangements are involved in the aqueous solvation reorganization in the first proton transfer step? The importance of solvent reorganization in the immediate vicinity of the hydrated excess proton in water has been stressed by Newton and Ehrenson²⁴ in their early work on the hydrated clusters of H_3O^+ and proton transfer within them. In this subsection, we study this aspect of the HCl acid ionization process.

We begin with a cluster calculation. By using the model potentials developed in section II.C, the cluster structure of eight external waters energetically minimized with the ionized system **2** is computed by the conjugate gradient optimization method³⁷ with the initial solvent molecules' configuration of the neutral cluster **1**. The observed characteristics of the structure change from **1** to **2** are summarized as follows: (i) the oxygen atoms in the external waters shrink slightly to the solute by 0.1–0.2 Å. On the other hand, the hydrogen atoms in the external waters have rather large displacements, in such a way that either the molecular orientational dipole or the OH local dipole reorganizes to stabilize the ion pair; (ii) in particular, the external water molecule that had been initially by hydrogen bonded to the oxygen atom of the neutral H_2O_a turns away from the hydronium ion H_3O_a^+ (Figure 8). This can be understood in terms of the local electrostatic repulsion between the net positive charge of H_3O^+ and the local partial charge on the hydrogen atom of that particular water molecule. In short, the motion of the identified solvent water molecule is critical in the **1** → **2** proton transfer, playing a primary role in the change of coordination from 4 for H_2O in **1** to 3 for H_3O^+ in **2**.

Newton and Ehrenson²⁴ found with an *ab initio* RHF method that the first solvation shell of H_3O^+ can accommodate only

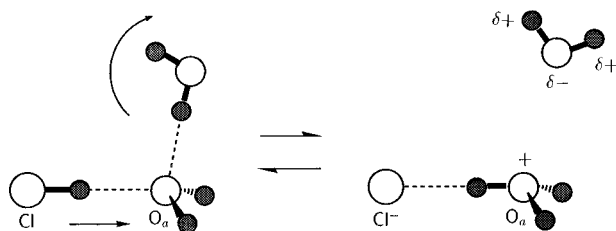


Figure 8. Schematic illustration of the possible reaction-promoting motion of a water molecule in the vicinity of the proton-accepting water H_2O_a , in the first proton transfer step $1 \rightarrow 2$.

three H_2O molecules, a result consistent with much chemical evidence^{4,58,59} and subsequent calculations.⁶⁰ Neither the “hydrogen-bonded” nor “charge-dipole” configurations of the fourth water molecule gave stabilization. On the other hand, Karlström²⁶ has recently reported a stable (by ~ 4 kcal/mol) charge-dipole configuration by *ab initio* RHF calculations with different basis sets. Our model potential gives a bound charge-dipole configuration (see below). Common in all the three works including ours is the local electrostatic repulsion between H_3O^+ and the local OH dipole of the fourth H_2O molecule, resulting in a primary coordination number of 3 for H_3O^+ (although our system is different, containing a chloride anion in the vicinity of the hydronium ion).

While the drastic changes in the local electrostatic interactions in the nearest-neighbor solvation included in the cluster calculation above will play the significant role, long-range interactions and correlations in the aqueous solvent may also couple to the reaction and should be taken into consideration. To explore this, a number of solution calculations were carried out by the Monte Carlo simulation. Figure 9 shows the energetic and configurational distributions in solution phase of a specific water molecule in the vicinity of the oxygen electron lone pair of H_2O_a or H_3O_a^+ . In the neutral state **1**, a linear hydrogen bonding is seen, whereas a charge-dipole type configuration of $\text{H}_3\text{O}_a^+ - \text{H}_2\text{O}$ with a binding energy distributed around ~ -4 kcal/mol is found for the state **2**. At the crossing point $\Delta E_{12} = 0$, that specific water is very weakly bound in a configuration rather similar to the charge-dipole type but noticeably away from the O_a atom. The solute–solvent interaction energy is smaller in the intermediate state, and consequently that particular water is pulled out from the reacting system into hydrogen-bond interaction with other external waters in the transition state region, and it clearly plays a central role in the reaction coordinate and the solvent activation process.⁶²

IV. Second Proton Transfer Step

Figures 10 and 11 display the corresponding solvent free energy curves and proton transfer potentials calculated for the second proton transfer $2 \rightarrow 3$. The appropriate solvent coordinate is now ΔE_{23} [cf. eq 2.2]. Here the O–O distance is taken to be 2.56 \AA , which is the equilibrium distance for $\text{H}_3\text{O}^+ - \text{H}_2\text{O}$ in the $\text{H}_3\text{O}^+(\text{H}_2\text{O})_3$ cluster. As will be seen below, this separation in solution is slightly higher in free energy, by 0.5 kcal/mol, than the $\text{H}_2\text{O} - \text{H}_2\text{O}$ equilibrium value (in a $(\text{H}_2\text{O})_5$ cluster) of 2.83 \AA . We believe that this reflects the influence of the bulk water solvent favoring a larger $\text{H}_3\text{O}^+ - \text{H}_2\text{O}$ separation than in a $\text{H}_3\text{O}^+(\text{H}_2\text{O})_3$ cluster.

It is seen in Figure 11 that the second proton transfer is adiabatic: the ground proton vibrational level is above the proton barrier in Figure 11b. But now in contrast to the first transfer $1 \rightarrow 2$ (cf. Figure 6), activation in the solvent is required, and an estimate of the activation energy which takes account of the quantized proton vibrational level is $\Delta G_{23}^\ddagger = 0.9$ kcal/mol

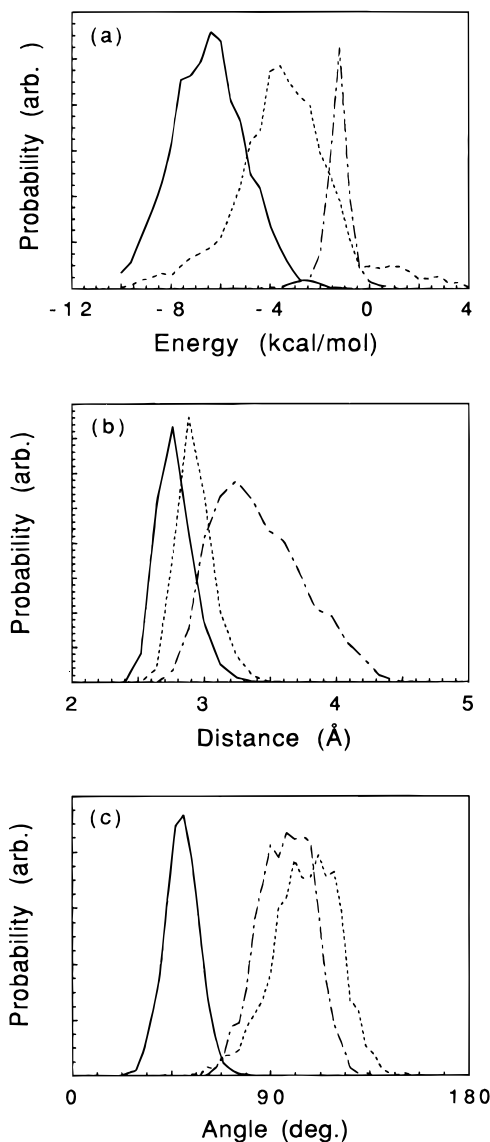


Figure 9. Energetic and configurational distributions of the specific water examined in Figure 8: (a) the $\text{H}_2\text{O} - \text{H}_2\text{O}_a$ (or H_3O_a^+) pair interaction energy, (b) the O– O_a distance, and (c) the angle between the O– O_a direction and the external water molecule's dipole moment direction. Solid, dashed, and dash-dot curves correspond to the reactant **1**, the product **2**, and the crossing point $\Delta E_{12} = 0$, respectively.

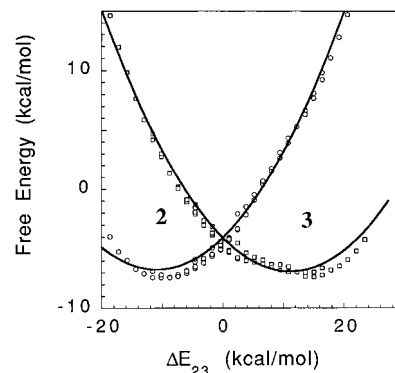


Figure 10. Same as Figure 3, but here for the second proton transfer $2 \rightarrow 3$ with the O–O distance 2.56 \AA . The solvent coordinate is ΔE_{23} .

(Figure 14, to be discussed below). This second transfer is nearly thermodynamically neutral, with an estimated reaction free energy of ΔG_{23} of only -0.2 kcal/mol. The solvent reorganization energy is 11.0 kcal/mol. The Monte Carlo

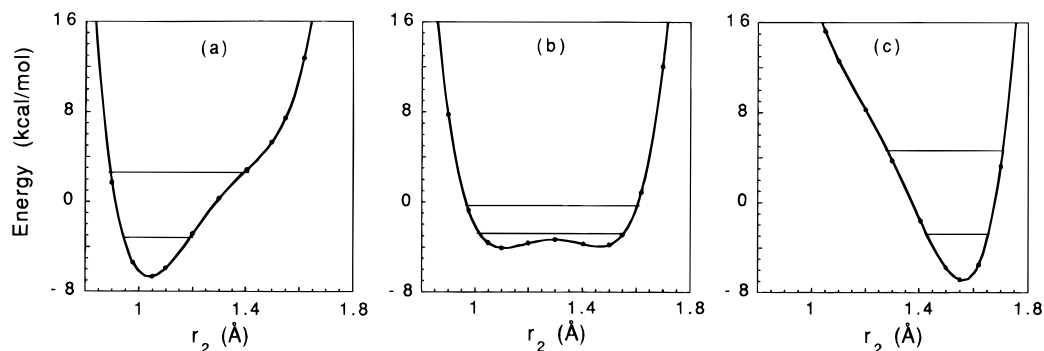


Figure 11. Same as Figure 4, but here for the second proton transfer $2 \rightarrow 3$ with the O—O distance 2.56 Å.

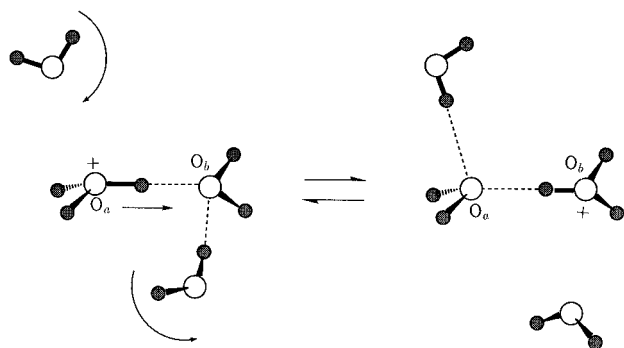


Figure 12. Schematic illustration of the possible reaction-promoting motion of two water molecules in the vicinity of H_2O_a and H_2O_b , for the second proton transfer step $2 \rightarrow 3$.

sampled points of the free energy curves are again will approximated by parabolas with the rms deviation of 1.02 kcal/mol.

We see in Figures 10 and 11 that the postulated scheme of section I (Figure 1) is appropriate also for the second proton transfer between H_3O^+ and H_2O . In this case, the proton affinities of the two proton sites are almost the same. The reaction is thus not usefully regarded in “covalent versus ionic” terms as was the case for the first proton transfer, but rather is similar to a (symmetric) charge-shift reaction. The polar aqueous solvation prefers a proton localized at either of the H_3O^+ sites, giving asymmetric proton potential wells at either site (Figure 11a,c), in the equilibrium reactant or product states. The transition between the two equilibrium polarization states requires activation in the solvent coordinate (Figure 10), and there is an intermediate crossing point that gives a symmetric proton potential (Figure 11b).

A rearrangement of the water molecule in the vicinity of H_2O_b or H_3O_b^+ , which is similar to the one discussed in section III.B, is found for the second proton transfer step in the nearest-neighbor solvation cluster in Figure 2: the water molecule hydrogen bonded to the neutral $\text{H}_2\text{Oz3b}$ in state 2 turns away from H_3O_g^+ in state 3, due to the critical change of the local electrostatic interaction. In addition, the water molecule in the vicinity of H_3O_a^+ in a charge-dipole type configuration in state 2 comes back to hydrogen bond to H_2O_a in state 3 (Figure 12).⁶¹ These water rearrangement motions accommodating the primary hydration number change from 4 for H_2O to 3 for H_3O^+ are expected to play an important role for this step ($2 \rightarrow 3$) in the solution phase reaction and make a significant contribution to the reaction coordinate.

A comparison calculation is very instructive here to reveal the role of solute heavy atom reorganization to the proton transfer. If the O—O separation is *not* allowed to “reorganize” from the H_2O — H_2O equilibrium value of 2.83 Å, the proton transfer is found instead to be nonadiabatic tunneling (Figure

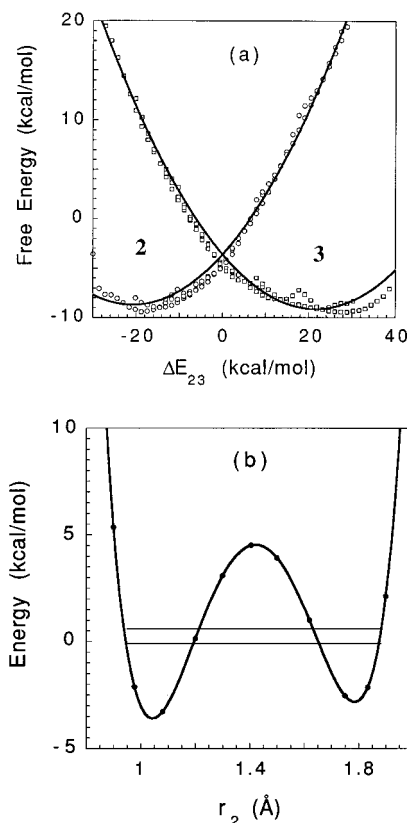


Figure 13. Same as (a) Figure 10 and (b) Figure 11b, but with the longer O—O distance 2.83 Å.

13). As seen by comparing Figures 11b and 13b, the proton transfer mechanism differs according to the relative position of the proton vibrational energy levels versus the proton potential barrier, which is quite sensitive to the O—O distance. The small (0.27 Å) change in the heavy atoms’ separation affects the potential of the transferring proton significantly, and thus nuclear reorganization plays a key role in this second transfer, as now discussed in more detail.⁶³

The free energy change associated with the O—O reorganization is found to be 0.5 and 0.9 kcal/mol for the states 2 and 3, respectively—these small values come from a cancellation between the solute internal energy gains and the solute—solvent and solvent—solvent interaction energy costs. For the large O—O distance, the activation and the reaction free energies—taking account of the proton vibrational level—and the solvent reorganization energy are 4.2, −0.6, and 21.2 kcal/mol, respectively (Figures 13a and 14). The free energy curves for the small and large O—O distances show that the transition state for the former is lower in energy than that for the latter by 2.7 kcal/mol (Figure 14), providing a strong bias against reaction at the larger O—O separation. In nearly thermoneutral processes

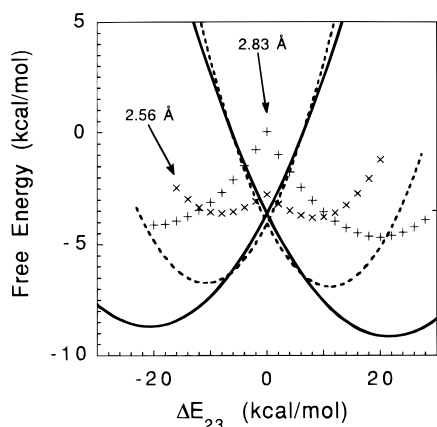


Figure 14. Same as Figure 6, but for the second proton transfer step $2 \rightarrow 3$ in the solvent coordinate ΔE_{23} .

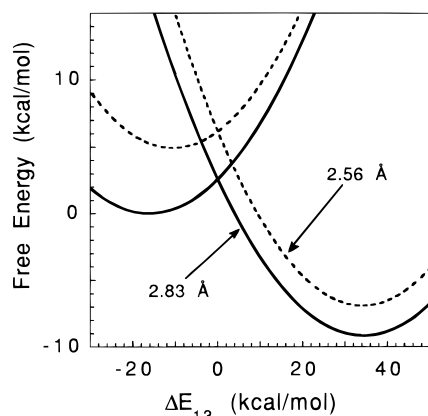


Figure 15. Same as Figure 6 (and 14), but for the concerted double proton transfer pathway $1 \rightarrow 3$ in the solvent coordinate ΔE_{13} . Only the diabatic free energy curves are shown.

such as these, the (diabatic) solvent activation energy is roughly proportional to the solvent reorganization energy; thus, these energy costs are smaller for the smaller proton shift. The adiabatic curves in Figure 14 show that the activation energy for the smaller O—O distance is even smaller compared to the larger O—O case.

Finally, Figure 13b shows that the passage through the diabatic crossing point in Figure 13a for the disfavored large O—O separation is not adiabatic but rather is tunneling, as noted above. Thus, the proton-tunneling probability (estimated in section VI to be 0.21) at the crossing point is another factor which further biases the reaction path against proton transfer at the larger O—O separation.

V. Concerted versus Stepwise Pathways

We have assumed throughout that the stepwise transfer ($1 \rightarrow 2 \rightarrow 3$) of the protons in Scheme 1 is the operative mechanism. We now examine the issue of this stepwise versus a concerted ($1 \rightarrow 3$) proton transfer by calculation of the free energy curves for the concerted double transfer, now in the solvent coordinate ΔE_{13} (see eq 2.2). For this purpose, we do not carry the calculations all the way to the adiabatic free energy curves. Instead we limit ourselves to a more restricted diabatic treatment, which is nonetheless sufficient to clarify the issue.

When the O—O distance is taken to be the $\text{H}_2\text{O}-\text{H}_2\text{O}$ equilibrium value of 2.83 Å, the activation energy for $1 \rightarrow 3$ in the ΔE_{13} coordinate is 2.6 kcal/mol, which is noticeably higher than that of the stepwise $1 \rightarrow 2$ transfer discussed above. This is shown in Figure 15. The $1 \rightarrow 3$ reorganization energy is computed to be 25.2 kcal/mol, which is larger than those for 1

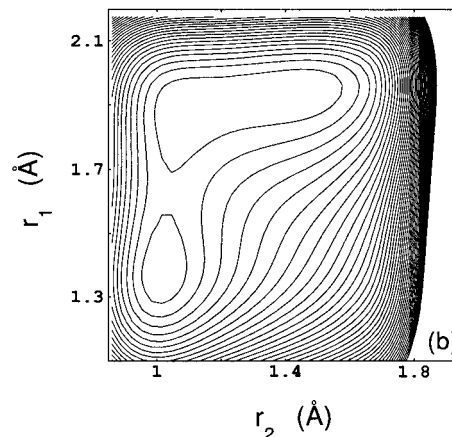
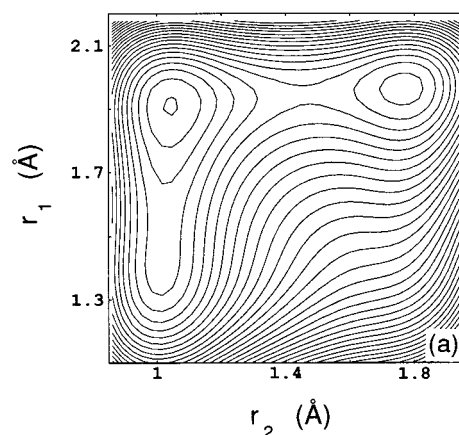


Figure 16. Proton potential surface evaluated at $\Delta E_{13} = 0$ at the O—O distance of (a) 2.83 Å and (b) 2.56 Å. Contour spacing is 2.5 kcal/mol.

$\rightarrow 2$ and $2 \rightarrow 3$. This (first) strong bias against a concerted transfer is general and robust against the numerical uncertainty in the simulation. It can be qualitatively understood in terms of the larger reorganization free energy for the solvent required for the large charge separation in $1 \rightarrow 3$, versus the smaller reorganization costs for the less drastic charge separations in $1 \rightarrow 2$ and $2 \rightarrow 3$.⁶⁴

Moreover, as displayed in Figure 16a, the proton potential surface at $\Delta E_{13} = 0$ has a high barrier along the r_2 direction, similar to the case for the $2 \rightarrow 3$ step with the O—O distance of 2.83 Å. This shows a (second) bias against the concerted pathway.

The importance of the reorganization of the O—O distance for the proton transfer along r_2 was emphasized in section IV. In the neutral state, the O—O compression has a free energy cost of ~ 5 kcal/mol. The free energy curves in the ΔE_{13} coordinate with the shorter O—O distance of 2.56 Å are computed and found to involve an activation energy of as large as 6.2 kcal/mol including the energy cost for the O—O compression (Figure 15). This portrays another (third) bias against the concerted pathway.

Figure 16b displays the proton potential surface at $\Delta E_{13} = 0$ with the smaller O—O distance 2.56 Å. Here the barrier along the r_2 direction is lowered considerably; however, the diagonal direction of (r_1, r_2) involves high energy compared to the stepwise-like pathway on the surface. This (fourth) bias against the diagonal pathway can be qualitatively understood as follows. We have discussed throughout that the proton transfer is pictured in terms of the proton potential asymmetry modulation by the solvent polarization fluctuation. For example, in the first step $1 \rightarrow 2$, the energy cost associated with the proton transfer which

comes from the proton affinity difference between Cl^- and H_2O is compensated by (or competes with) the free energetic stabilization of the ion pair via solvation by the polar aqueous medium. According to this picture, the midpoint of the diagonal pathway in Figure 16b is expected to be unstable because it involves the cost of breaking two bonds, but does not gain solvation energy, due to the delocalized charge distribution of the intermediate structure.

To summarize, we conclude that the concerted pathway for the double proton transfer in Scheme 1 is unfavorable compared to the stepwise mechanism.⁶⁵ We believe that the qualitative arguments here should also apply for general proton transport processes in water. Such a stepwise proton transfer scenario is in contrast with descriptions in which, e.g., an existence of a solitonic motion⁶⁶ is suggested.

VI. Solvent Electron Polarization Effects

A. Impact on Proton Barrier and Vibrational Levels. The present calculations take no explicit account of the solvent electronic polarization. At and near the crossing points of the diabatic free energies in the solvent coordinate, the proton potentials were computed under the fixed field of the solvent point charges. This neglects the correlation between the electrons in the solvent molecules and the solute electronic structure change associated with the proton transfer. In particular, the way the solvent electronic polarization solvates the intermediate electronic structure at the proton barrier region may alter the barrier height and thus the adiabaticity of the proton motion. A model for the problem was recently given by Kim and Hynes,⁶⁷ which considers charge localized VB states correlating to the quantized dielectric continuum field of the solvent electronic polarization, over the entire range of the resonance electronic coupling between the VB states. They discussed two limiting cases, i.e. the self-consistent (SC) and the Born–Oppenheimer (BO) limits, and an exact theory within the framework of the model. A key concept is the competition between the time scales of the solvent electronic polarization and the electronic resonance of the solute VB states.^{67,68} This issue has been discussed recently⁹ for the large electronic coupling situation of proton transfer, and we give here only an abbreviated (but sufficient) discussion.

The computational procedure employed here roughly corresponds to the SC limit in a sense that the fixed classical field of the solvent molecular point charges see the delocalized electronic distribution of the (quantum chemically treated) solute molecules in the proton barrier region. In the BO limit, on the other hand, the solvent electronic polarization fully solvates the individual component solute electronic VB states at every point of the proton coordinate and would lead to greater stabilization in the proton barrier region than an SC treatment. Aqueous proton transfers such as the present are expected to be closer to the BO limit, considering the typical “resonance energy” for the VB states for the proton transfer (~ 1 eV)⁷ and the time scale of the electronic polarization in the solvent water (~ 7.4 eV in energy).⁶⁷ Thus, the qualitative trend would be that a full account of the solvent electronic polarization lowers the proton barrier compared to the present results.⁶⁹ Although quantitative description of this issue based on microscopic molecular models—at a level consistent with the present one for the solute electronic structures—is not attempted here, a rough estimate suggests, for example for the first step $1 \rightarrow 2$, ~ 1.4 kcal/mol change of the proton barrier height and a smaller effect on the proton vibrational levels,⁷⁰ which is what is important for the reaction barrier. This indicates that the proton transfers would in fact be even more adiabatic (or nontunneling) than we have

TABLE 3: Landau–Zener Parameters

step	$2 \rightarrow 3^a$	$2 \rightarrow 3^b$	$1 \rightarrow 2^c$	$1 \rightarrow 2^d$	$1 \rightarrow 2^e$	$1 \rightarrow 2^f$
C (kcal/mol)	0.34	1.23	0.67	0.87	0.95	1.19
P_{LZ}	0.12	0.90	0.47	0.66	0.73	0.87
$2P_{\text{LZ}}/(1 + P_{\text{LZ}})$	0.21	0.95	0.64	0.80	0.84	0.93

^{a–f} The O–O distance in *a* is 2.83, in *b* is 2.56, and in *c–f* is 2.83 Å, respectively. The Cl–O distance in *a–d* is 2.96 and in *e, f* is 2.91 Å. The proton potentials for *d* and *f* are obtained by lowering the proton barriers of *c* and *e* respectively by 1.4 kcal/mol. See the text for details.

found for the first and the second transfer steps displayed in Figures 4b (5b) and 11b, respectively. This last point will be further discussed in the next subsection.

B. Adiabaticity from a Curve-Crossing Model. In all of the preceding, we have taken the location of the zero-point proton vibrational level above the proton transfer barrier as the indicator of adiabaticity. We now examine this issue from a dynamical viewpoint.

For the tunneling case, the proton transfer mechanism is well characterized by the “proton coupling” C which is defined here by half the energy splitting of the lowest two proton vibrational levels held in each double well (cf. Figure 13b). In this case, the reaction rate constant is described by a perturbation expansion in C giving a golden rule rate formula,^{6,71} which has a form similar to that of outer-sphere electron transfer reactions.^{13b} The idea is extended^{8,9,18c} to the large coupling (adiabatic) limit by employing a semiclassical Landau–Zener curve-crossing model.⁷² The key quantity which characterizes the reaction adiabaticity and mechanism is the Landau–Zener transition probability given by

$$P_{\text{LZ}} = 1 - \exp\left(-\frac{2\pi C^2}{\hbar\sqrt{\langle\dot{E}^2\rangle}}\right) = 1 - \exp\left(-\frac{2\pi C^2}{\hbar\Omega\sqrt{2k_{\text{B}}T\Delta G_{\text{r}}}}\right) \quad (6.1)$$

where by velocity of the curve crossing is represented by its thermal average $\langle\dot{E}^2\rangle^{1/2}$, and thus by the solvent frequency Ω and the reorganization energy ΔG_{r} . P_{LZ} represents the transition probability per crossing. When any quantum interface and friction effects are neglected,^{72,73} the net probability for the passage to the product well—when all energetic requirements for the reaction are satisfied—is given by

$$P = 2P_{\text{LZ}}/(1 + P_{\text{LZ}}) \quad (6.2)$$

These parameters are computed for the steps $1 \rightarrow 2$ and $2 \rightarrow 3$ are listed in Table 3.

It is seen that for the tunneling case ($2 \rightarrow 3$ with the O–O distance 2.83 Å, Figure 13), which we have argued in section IV to be already disfavored on energetic grounds, P_{LZ} and P are small: $P_{\text{LZ}} = 0.12$ and $P = 0.21$. Interestingly, P_{LZ} and P are slightly smaller than unity for the $2 \rightarrow 3$ step with the favored smaller O–O distance (2.56 Å), where the proton ground level is above the proton barrier top (Figure 11b). This means that this proton transfer is not purely “adiabatic” according to the curve-crossing concept. This is an interesting feature of the solvent water with a relatively fast ($\Omega \approx 400$ cm^{−1}) fluctuation of the solvent librational reorganization,⁷⁴ which tends to suppress P_{LZ} and P (cf. eq 6.1). This can be compared with, e.g., the polar CH_3Cl solvent which gives $P_{\text{LZ}} \sim 1$ for an adiabatic acid ionization with a comparable value of the proton coupling.⁹ However, this small dynamic nonadiabaticity would

be expected to disappear for the reasons now discussed in connection with the $1 \rightarrow 2$ transfer.

The adiabaticity parameter P_{LZ} for the first proton transfer step $1 \rightarrow 2$ is computed to be 0.47 at the Cl–O distance 2.96 Å (Figure 4b). The ground and the first excited vibrational levels in Figure 4b suggest that while this proton transfer is certainly not a “deep-tunneling” event, it is not necessarily a “pure-adiabatic” process either. However, there are several reasons, including the arguments for the smaller Cl–O distance results (Figure 5) in section III.A, to expect that any nonadiabaticity will actually be less pronounced than this. First, the discussion in section VI.A indicates that an explicit account of the solvent electronic polarization will lower the proton barrier and consequently increase the adiabaticity polarization will lower the proton barrier and consequently increase the adiabaticity parameter P_{LZ} and P . We have examined this effect by modifying the proton potential of Figure 4b by scaling the barrier region so that the barrier height is lowered by 1.4 kcal/mol (see section VI.A and ref 70). This makes the ground proton vibrational level slightly (0.4 kcal/mol) above the barrier top, and the adiabaticity is found to increase considerably: $C = 0.87$ kcal/mol, $P_{LZ} = 0.66$, and $P = 0.80$. Furthermore, P_{LZ} (and P) may be sensitive to the Cl–O distance. As in section III.A (Figure 5), we examine a slight (0.05 Å) compression of the Cl–O distance and find a significant increase of the adiabaticity parameter: $P_{LZ} = 0.73$ and $P = 0.84$ with $C = 0.95$ kcal/mol. When the proton barrier is again lowered by 1.4 kcal/mol for this slightly compressed system, the adiabaticity is further increase: $P_{LZ} = 0.87$ and $P = 0.93$ with $C = 1.19$ kcal/mol. Finally, since the solvent barriers for these processes are nonexistent or small, there will likely to be considerable barrier recrossing.^{13d,75} In such a case, the recrossings will tend to increase the effective P .⁷⁶ Therefore, to conclude, an assortment of possible impacts of going beyond the present modeling indicates that the proton transfer between HCl and H₂O is most likely to be fully adiabatic, although we cannot absolutely rule out small dynamical nonadiabatic effects.

VII. Concluding Remarks

We have presented here the results of a study of the mechanism of the acid ionization of HCl in water. The picture that emerges is that the HCl ionization is a consecutive set of quantum adiabatic, nontunneling, proton transfers. The first transfer involves an almost activationless solvent reorganization to a contact Cl[−]–H₃O⁺ ion pair, with an accompanying reaction free energy of −6.7 kcal/mol. The second transfer to produce a solvent-separated ion pair is slightly activated in a solvent coordinate and is approximately thermoneutral. A key component in the required solvent reorganization in each step is a solvent water molecule rearrangement to accommodate the change of coordination number of the proton-accepting water from 4 (for H₂O) to 3 (for H₃O⁺). The two proton transfers occur in a stepwise fashion; there are assorted strong biases against a concerted pathway. The two proton transfers follow a nonequilibrium solvation path in their respective solvent coordinate.

The overall experimental reaction free energy of HCl ionization in water eq 1.1 is⁵⁶ −8 to −10 kcal/mol. While no simulations have been performed for the remaining passage from the solvent-separated ion pair structure **3** in Scheme 1 to the fully separated ions, a dielectric continuum (screened Coulomb) estimate suggests that process involves only a very small (less than 1 kcal/mol) overall free energy change in the high dielectric constant (~80) aqueous solution; when a proton of H₃O_b⁺ in **3** is further transferred to the next adjacent water, the first solvation

shells for each of Cl[−] and H₃O⁺ will be completed. The dielectric screening for these “dressed” hydration clusters Cl[−](H₂O)_n ($n = 4-6$) and H₃O⁺(H₂O)₃ should be very efficient in aqueous solution. We expect, however, that there can be small barriers in a solvent coordinate—much like that in the second step $2 \rightarrow 3$ above⁷⁷—along the pathway, as well as nuclear reorganization of O–O distances to assist the adiabatic proton transfer. As argued in section IV, we anticipate these processes to be stepwise—rather than concerted and solitonic—in character.

Because our estimated simulation uncertainty is rather less than one kilocalorie per mole, we anticipate that the qualitative picture stated above is robust, e.g., the adiabatic first proton transfer $1 \rightarrow 2$ is at most nearly activationless, and the major part of the reaction exothermicity is gained in this first step. From this contact ion pair state to the fully separated ions, the intramolecular energy would not change drastically, in a sense that the chemical species are always Cl[−] and H₃O⁺ in water.⁷⁸ By employing again a dielectric continuum estimate, the separation of the contact ion pair (at intermolecular distance ≈3 Å) to infinity would cost less than 2 kcal/mol in free energy. This consideration, though quite simplified, qualitatively supports the computed thermoneutrality of the second step $2 \rightarrow 3$, as well as the conclusion above on the first step.

Since the solvent barriers for the first two steps are either negligible or small, there could well be considerable barrier-recrossing effects which would need to be taken into account in the computation of reaction rate constants.^{13d,75,79,80} In particular, the $1 \rightarrow 2$ proton transfer step could be diffusive in character, with multiple solvent barrier recrossings associated with the dynamics of the fourth H₂O molecule rearrangement noted in section III.B. Also, since the $1 \rightarrow 2$ transfer evidently has a negligible barrier, there is likely to be the necessity of time dependent rate constants to describe the nonexponential kinetics, with the solvent dynamics playing a significant role.^{13d,81,82} This feature—as with the dynamic curve-crossing aspects discussed in section VI.B—enriches, but would not alter, the energetic pathways above. Neglecting these considerations, the time scales for the first and the second PT steps are estimated to be 0.1 and 0.4 ps, respectively, by using a semiclassical rate formula, $k = 2P_{LZ}/(1 + P_{LZ})(\Omega/2\pi) \exp(-\Delta G^\ddagger/k_B T)$.

We can also compare the proton potential surfaces in the small cluster (Figure 2) and in the bulk (~130 externals) solvation calculations in order to clarify what might be expected in gas phase clusters HCl(H₂O)_n. As seen in Figure 17, the reorganization of only eight external waters in the cluster gives stable minima for each of the states **1–3**. Quantitatively, each minimum is deeper in the solution phase. But still the qualitative features of the potential surfaces are well represented by solely the nearest-neighbor reorganization. This suggests that clusters HCl(H₂O)_n somewhat larger than have been previously examined experimentally^{11a} could display ion pair formation.⁸³

In view of the predicted rapid and exothermic character of the HCl ionization to a contact ion pair in water that follows from the calculations within,⁸⁴ this system is evidently not the most accessible to direct experimental study of the reaction process, although this should certainly be explored experimentally. This rapidity may account for the absence of experimental results for HCl ionization time scales. One way to slow the thermal reaction to bring its initial steps within the window of ultrafast spectroscopy⁸⁵ might be to carry out the reaction in supercritical water.⁸⁶ The effective polarity of this solvent, while variable, is much lower than that of liquid water,⁸⁷ and considerably less stabilization of the ion pairs should result.⁸⁸

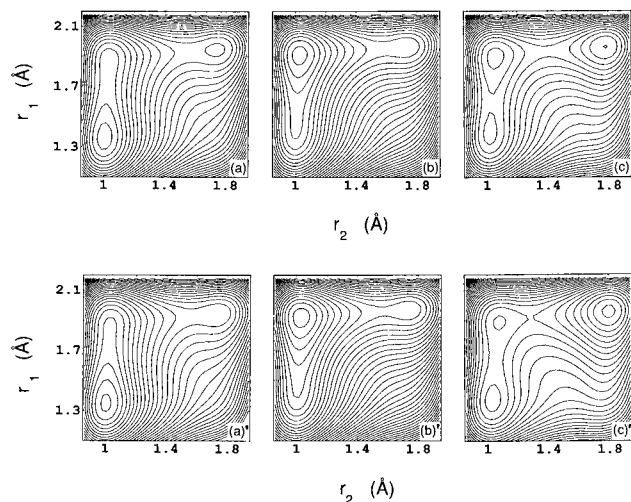


Figure 17. Comparison of the proton potential surface for the systems 1–3 (a)–(c) in the cluster with eight external waters (cf. Figure 2) and (a')–(c') in bulk (~130 externals) equilibrium solvation. The configuration of the external waters in the cluster is reorganized to each charge distribution of the states 1–3 (see sections II.B and III.B). The solvent configuration for (a')–(c') is sampled in the course of the Monte Carlo simulation (section III.A). Contour spacing is 2.5 kcal/mol.

Another route to a slower acid ionization would be the study of a weaker acid, e.g., HF ($pK_a \approx +3$),¹ in liquid water;¹⁷ this should also reveal, when viewed in the reverse recombination sense, the short-range aspects of the reaction dynamics inaccessible to prior experimental techniques.⁴ Such endothermic dissociations also provide a potential arena for infrared laser-induced acid ionizations.⁸⁹ The methods of the present work are being applied to study the HF ionization.

The considerations outlined here can also be employed to study⁹⁰ the issue of HCl ionization at ice surfaces in connection with ozone depletion.⁹¹

Finally, we have examined the various site charges in the trimer solute for the transfer $1 \rightarrow 2$ in solution at the approximate transition state configuration $\Delta E_{12} = 0$. Comparison of these with those of Table 1 for the reactant and product gives the following pattern in the $1 \rightarrow \ddagger \rightarrow 2$ process: Cl ($-0.417 \rightarrow -0.654 \rightarrow -0.846$), H₁ ($0.298 \rightarrow 0.321 \rightarrow 0.327$), O_a ($-0.975 \rightarrow -0.672 \rightarrow -0.593$), H₂ = H₃ ($0.542 \rightarrow 0.485 \rightarrow 0.543$). It is especially intriguing to note that the patterns of the growth of the Cl negative charge, the decrease of the O negative charge, and the approximate constancy of the H charge are consistent with a Mulliken-type charge transfer picture.^{7,12,92} We will pursue this aspect and related considerations for the second proton transfer step in more detail elsewhere.

Acknowledgment. This work was supported in part by an NIH Shannon Award and by Grants NSF CHE88-07852, NSF CHE93-12267, and NSF CHE97-00419. We also acknowledge support from Pittsburgh Supercomputing Center. K.A. was partly supported by a Fellowship of the Japan Society for the Promotion of Science. We thank Dr. A. Staib for fruitful discussions.

References and Notes

- (1) Bell, R. P. *The Proton in Chemistry*; Chapman and Hall: London, 1973. *Proton Transfer Reactions*; Caldin, E. F., Gold, V., Eds.; Chapman and Hall: London, 1975. Bell, R. P. *The Tunnel Effect in Chemistry*; Chapman and Hall: London, 1980. *Isotope Effects in Organic Chemistry*; Buncl, E., Lee, C. C., Eds.; Elsevier: Amsterdam, 1976; Vol. 2. Hibbert, F. *Adv. Phys. Org. Chem.* **1986**, *22*, 113. Hibbert, F. *Ibid.* **1990**, *26*, 255. Westheimer, F. H. *Chem. Rev.* **1961**, *61*, 265.

- (2) (a) Kosower, E. M.; Huppert, D. *Annu. Rev. Phys. Chem.* **1986**, *37*, 127. Kreevoy, M. M.; Truhlar, D. G. In *Rates and Mechanisms of Reactions*, 4th ed.; Bernasconi, C. F., Ed.; Wiley: New York, 1986; Chapter 1. Ratajczak, H. In *Electron and Proton Transfer Processes in Chemistry and Biology*; Müller, A., Ratajczak, H., Junge, W., Diemann, E., Eds.; Elsevier: Amsterdam, 1992. (b) *Proton Transfer in Hydrogen-Bonded Systems*; Bountis, T., Ed.; Plenum: New York, 1993. (c) See also the special issues on proton transfer: *Chem. Phys.* **1989**, *136* (2). *J. Phys. Chem.* **1991**, *95*, (25).
- (3) Jencks, W. P. *Catalysis in Chemistry and Enzymology*; McGraw-Hill: New York, 1969. van Duijnen, P. Th. *Enzyme* **1986**, *36*, 93. Bender, M. L. *Mechanisms of Homogeneous Catalysis from Protons to Proteins*; Wiley: New York, 1971. Fersht, A. *Enzyme Structure and Mechanisms*; W. H. Freeman: New York, 1985. Gandour, R. D.; Schowen, R. L. *Transition States of Biochemical Processes*; Plenum: New York, 1978. Klinman, J. P. *CRC Crit. Rev. Biochem.* **1981**, *10*, 39. Menger, F. *Acc. Chem. Res.* **1993**, *26*, 206. Gutman, M.; Nachliel, E. *Biochim. Biophys. Acta* **1990**, *391*, 1015.
- (4) Eigen, M.; Kruse, W.; De Mayer, L. *Prog. React. Kinet.* **1964**, *2*, 285. Eigen, M. *Angew. Chem., Int. Ed. Engl.* **1964**, *3*, 1. Eigen, M. *Pure Appl. Chem.* **1963**, *6*, 97.
- (5) Albery, W. J. *Prog. React. Kinet.* **1967**, *4*, 353. Maréchal, Y. In ref 2b.
- (6) Borgis, D.; Lee, S.; Hynes, J. T. *Chem. Phys. Lett.* **1989**, *162*, 19. Borgis, D.; Hynes, J. T. *J. Chem. Phys.* **1991**, *94*, 3619; *Chem. Phys.* **1993**, *170*, 315.
- (7) Juanós i Timoneda, J.; Hynes, J. T. *J. Phys. Chem.* **1991**, *95*, 10431.
- (8) Borgis, D.; Hynes, J. T. *J. Phys. Chem.* **1996**, *100*, 1118.
- (9) Staib, A.; Borgis, D.; Hynes, J. T. *J. Chem. Phys.* **1995**, *102*, 2487.
- (10) Ando, K.; Hynes, J. T. In *Structure and Reactivity in Aqueous Solution: Characterization of Chemical and Biological Systems*; Cramer, C. J., Truhlar, D. G., Eds.; ACS Books: Washington DC, 1994; *J. Mol. Liq.* **1995**, *64*, 25.
- (11) (a) Legon, A. C.; Willoughby, L. G. *Chem. Phys. Lett.* **1983**, *95*, 449. (b) Bacskaý, G. B. *Mol. Phys.* **1992**, *77*, 61. Bacskaý, G. B.; Kerdrón, D. I.; Hush, N. S. *Chem. Phys.* **1990**, *144*, 53. (c) Chipot, C.; Gorb, L. G.; Rivail, J.-L. *J. Phys. Chem.* **1994**, *98*, 1601. Rivail, J.-L.; Antonczak, S.; Chipot, C.; Ruiz-López, M. F.; Gorb, L. G. In *Structure, Energetics, and Reactivity in Aqueous Solution*; Cramer, C. J., Truhlar, D. G., Eds.; ACS Books: Washington DC, 1994.
- (12) Warshel, A.; Weiss, R. M. *J. Phys. Chem.* **1980**, *102*, 6218. Warshel, A.; Russel, S. *J. Am. Chem. Soc.* **1986**, *108*, 6569. Warshel, A. *Computer Modeling of Chemical Reactions in Enzymes and Solutions*; Wiley: New York, 1991.
- (13) (a) Marcus, R. A. *Annu. Rev. Phys. Chem.* **1964**, *15*, 155. Newton, M. D.; Sutin, N. *Ibid.* **1984**, *35*, 437. (b) Ulstrup, J. *Charge Transfer Processes in Condensed Media*; Springer-Verlag: Berlin, 1979. For representative simulation studies, see e.g.: (c) Warshel, A.; Hwang, J.-K. *J. Chem. Phys.* **1986**, *84*, 4938. Hwang, J.-K.; Warshel, A. *J. Am. Chem. Soc.* **1987**, *109*, 715. Kuharski, R. A.; Bader, J. S.; Chandler, D.; Spirk, M.; Klein, M. L.; Impey, R. W. *J. Chem. Phys.* **1988**, *89*, 3248. Kneifel, C. L.; Newton, M. D.; Friedman, H. L. *J. Mol. Liq.* **1994**, *60*, 107. (d) Fonseca, T.; Ladanyi, B. M. In *Ultrafast Reaction Dynamics and Solvent Effects: Experimental and Theoretical Aspects*; Gauduel, Y., Rossky, P. J., Eds.; AIP Press: New York, 1994.
- (14) Fonseca, T.; Kim, H. J.; Hynes, J. T. *J. Mol. Liq.* **1994**, *60*, 161. Kato, S.; Amatatsu, Y. *J. Chem. Phys.* **1990**, *92*, 7241.
- (15) Mathis, J. R.; Hynes, J. T. *J. Phys. Chem.* **1994**, *98*, 5445, 5460. For more typical examples of S_N1 reactions in which the electronic coupling is strong enough to obliterate any solvent barrier, see: Kim, H. J.; Hynes, J. T. *J. Am. Chem. Soc.* **1992**, *114*, 10508, 10528. Mathis, J. R.; Kim, H. J.; Hynes, J. T. *Ibid.* **1993**, *115*, 8248.
- (16) The degree to which this is also true for weaker acids—where the standard picture is most often applied—will be discussed in ref 17.
- (17) Ando, K.; Hynes, J. T. *Discuss. Faraday Soc.*, in press; Molecular Mechanism of HF Ionization in Water, to be submitted.
- (18) (a) Gillan, M. J. *Phys. Rev. Lett.* **1987**, *58*, 563. *J. Phys. C* **1987**, *20*, 3621. (b) Voth, G. A.; Chandler, D.; Miller, W. H. *J. Phys. Chem.* **1989**, *93*, 7009; *J. Chem. Phys.* **1989**, *91*, 7749. (c) Li, D. H.; Voth, G. A. *J. Phys. Chem.* **1991**, *95*, 10425. Lobaugh, J.; Voth, G. A. *Chem. Phys. Lett.* **1992**, *198*, 311; *J. Chem. Phys.* **1994**, *100*, 3039; **1995**, *104*, 2056. These papers can be consulted for a demonstration of how a path integral centroid approach capture a solvent activation component for a rate constant. (d) Azzouz, H.; Borgis, D. *J. Chem. Phys.* **1993**, *98*, 7361; *J. Mol. Liq.* **1994**, *61*, 17. (e) Ferrario, M.; Laria, D.; Ciccotti, G.; Kapral, R. *Ibid.* **1994**, *61*, 37.
- (19) Borgis, D.; Tarjus, G.; Azzouz, H. *J. Phys. Chem.* **1992**, *96*, 3188; *J. Chem. Phys.* **1992**, *97*, 1390. Laria, D.; Ciccotti, G.; Ferrario, M.; Kapral, R. *J. Chem. Phys.* **1992**, *97*, 378.
- (20) For earlier work on quantum proton transfers including some aspects of adiabatic transfer, see ref 13b and: German, E. D.; Kuznezov, A. M.; Dogonadze, R. R. *J. Chem. Soc., Faraday Trans. 2* **1980**, *76*, 1128. Krishtalik, L. I. *Charge Transfer Reactions in Electrochemical and Chemical Processes*; Plenum: New York, 1986.

- (21) The involvement of a similar situation—zero-point vibration over the proton barrier—has been recently implicated as an important energetic factor in some enzymatic reactions: Cleland, W. W.; Kreevoy, M. M. *Science* **1994**, 264, 1887. Cleland, W. W. *Biochemistry* **1992**, 31, 317. Gerlt, J. A.; Gassman, P. G. *Ibid.* **1993**, 32, 11943.
- (22) Scheiner, S. *Acc. Chem. Res.* **1985**, 18, 174; *J. Chem. Phys.* **1982**, 77, 4039; *J. Am. Chem. Soc.* **1981**, 103, 315.
- (23) Komatsuzaki, T.; Ohmine, I. *Chem. Phys.* **1994**, 180, 239.
- (24) Newton, M. D.; Ehrenson, S. *J. Am. Chem. Soc.* **1971**, 93, 4971. Newton, M. D. *J. Chem. Phys.* **1977**, 67, 5535.
- (25) Halle, B.; Karlstrom, G. *J. Chem. Soc., Faraday Trans. 2* **1983**, 79, 1047. Stillinger, F. H. In *Theoretical Chemistry. Advances and Perspectives*; Eyring, H., Henderson, D., Eds.; Academic Press: New York, 1978; Vol. 3.
- (26) Karlstrom, G. *J. Phys. Chem.* **1988**, 92, 1318.
- (27) Gandour, R. D.; Maggiora, G. M.; Schowen, R. L. *J. Am. Chem. Soc.* **1974**, 96, 6967.
- (28) A critical involvement of solvent water is also suggested for the tautomerization of 7-azaindole. See, e.g.: Chapman, C. F.; Maroncelli, M. *J. Phys. Chem.* **1992**, 96, 8430.
- (29) Dupuis, M.; Watts, J. D.; Villar, H. O.; Hurst, G. J. B. *HONDO Ver. 7.0. QCPE* **1987**, 544.
- (30) Möller, C.; Plesset, M. S. *Phys. Rev.* **1934**, 45, 618. Krishnan, R.; Frisch, M. J.; Pople, J. A. *J. Chem. Phys.* **1980**, 72, 4244.
- (31) Binkley, J. S.; Pople, J. A.; Hehre, W. J. *J. Am. Chem. Soc.* **1980**, 102, 939. Hehre, W. J.; Ditchfield, R.; Pople, J. A. *J. Chem. Phys.* **1972**, 56, 2252.
- (32) Dunning, T. H.; Hay, P. J. In *Methods of Electronic Structure Theory*; Schaefer, H. F., III, Ed.; Plenum: New York, 1977.
- (33) Urban, M.; Cernusak, I.; Kellö, V.; Noga, J. In *Methods in Computational Chemistry*; Wilson, S., Ed.; Plenum: New York, 1987.
- (34) Shavitt, I. In *Methods of Electronic Structure Theory*, Schaefer, H. F., III, Plenum: New York, 1977.
- (35) Spangler, D.; Williams, I. H.; Maggiora, G. J. *Comput. Chem.* **1983**, 4, 524.
- (36) Here the hydrogen bonds are not constrained to be linear, and C_s symmetry is imposed.
- (37) Jorgensen, W. L.; Chandrasekhar, J.; Madura, J.; Impey, R. W.; Klein, M. L. *J. Chem. Phys.* **1983**, 79, 926.
- (38) Allen, M. P.; Tildesley, D. J. *Computer Simulation of Liquids*; Clarendon: Oxford, 1987.
- (39) Owicki, J. C. *ACS Symp. Ser.* **1978**, 86, 159. Jorgensen, W. L.; Bigot, B.; Chandrasekhar, J. *J. Am. Chem. Soc.* **1982**, 104, 4584.
- (40) Neilson, G. W.; Enderby, J. E. *Annu. Rep. Prog. Chem., Sect. C* **1979**, 76, 185. Enderby, J. E.; Neilson, G. W. *Rep. Prog. Phys.* **1981**, 44, 38.
- (41) Newsome, J. R.; Neilson, G. W.; Enderby, J. E. *J. Phys. C: Solid State Phys.* **1980**, 13, L923. Cummings, S.; Enderby, J. E.; Neilson, G. W.; Howe, R. A.; Howells, W. S.; Soper, A. K. *Nature (London)* **1980**, 287, 714.
- (42) Clementi, E.; Barsotti, R. *Chem. Phys. Lett.* **1980**, 59, 21.
- (43) Mezei, M.; Beveridge, D. L. *J. Chem. Phys.* **1981**, 74, 6902.
- (44) Heinzinger, K.; Vogel, P. C. *Z. Naturforsch., A* **1976**, 31, 463. Vogel, P. C.; Heinzinger, K. *Ibid.* **1976**, 31, 463. Palinkas, G.; Riede, W. O.; Heinzinger, K. *Ibid.* **1977**, 32, 1137. Bopp, P.; Dietz, W.; Heinzinger, K. *Ibid.* **1979**, 34, 1424. Szasz, G. I.; Heinzinger, K. *Ibid.* **1979**, 34, 840.
- (45) Impey, R. W.; Madden, P. A.; McDonald, I. R. *J. Phys. Chem.* **1983**, 87, 5071.
- (46) Chandrasekhar, J.; Spellmeyer, D. C.; Jorgensen, W. L. *J. Am. Chem. Soc.* **1984**, 106, 903.
- (47) Appropriate account of the induced electronic polarization of the solvent was found to improve agreement of the calculated hydration number with the experimental. Dang, L. X.; Rice, J. E.; Caldwell, J.; Kollman, P. A. *J. Am. Chem. Soc.* **1991**, 113, 2481.
- (48) (a) King, G.; Warshel, A. *J. Chem. Phys.* **1990**, 93, 8682. (b) Ando, K.; Kato, S. *J. Chem. Phys.* **1991**, 95, 5966.
- (49) It is derived from the definition eqs 2.2–2.4 that the difference between the two diabatic free energy curves is precisely the solvent coordinate, i.e., $G_i(\Delta E_{ij}) - G_j(\Delta E_{ij}) = \Delta E_{ij}$, independent of whether the probability distribution is Gaussian or not. Thus, the curvatures of the two diabatic free energy curves must be the same when they are parabolic. See: Kakitani, T.; Mataga, N. *J. Phys. Chem.* **1985**, 89, 4752. Carter, E. A.; Hynes, J. T. *Ibid.* **1989**, 93, 2184. Tachiya, M. *Ibid.* **1989**, 93, 7050. Yoshimori, A.; Kakitani, T.; Enomoto, Y.; Mataga, N. *Ibid.* **1989**, 93, 8316. See also ref 48 for simulation studies and the following for connections to solvation free energies: Fonseca, T.; Ladanyi, B. M.; Hynes, J. T. *J. Phys. Chem.* **1992**, 96, 4085.
- (50) Non-Gaussian statistics might be important for proton transfer cases compared to electron transfer cases, due to the longer-ranged electrostatic potentials of the latter. The deviation from Gaussian behavior of the diabatic curves—the rms deviation of the Monte Carlo points from the fitted parabolas—found in the present system is as small as the simulation uncertainties (≤ 1 kcal/mol), which implies that the present system cannot be very non-Gaussian. But it should be noted that the harmonic diabatic curves are here used only as a guide to the ultimate calculation of the free energy curves.
- (51) Johnson, B. R. *J. Chem. Phys.* **1977**, 67, 4086. Roemelt, J. *Chem. Phys. Lett.* **1980**, 74, 263.
- (52) In simple VB terms (ref 7), this is due to the exponential dependence of the overlap between atomic orbitals, and thus the electronic coupling between VB states, on the internuclear distance.
- (53) It is convenient to consider the proton and the solvent coordinates in the same unit (dimension) by transforming to the mass-weighted ones. The mass of the solvent coordinate ΔE is given by $\mu = (2\Delta G_r \Omega^2)^{-1}$, where ΔG_r and Ω are the solvent reorganization energy and the associated frequency (see footnote 74 below), respectively. By mass weighting the coordinates to $m^{1/2}r_1$ and $\mu^{1/2}\Delta E$, where m is the reduced mass of the Cl–H coordinate r_1 , the length ratio of the ordinate and abscissa of Figure 7 is scaled to be about 15:1. This further supports the adequacy of the quantum adiabatic separation of the proton coordinate.
- (54) One might argue from inspection of Figure 7 that, from a classical perspective, $\Delta E = 0$ is an inferior choice for the transition state (TS) (note that we find a value very slightly shifted from this for the adiabatic free energy curves) and that the classical saddle point ($r_1 \approx 1.55$ Å, $\Delta E \approx 3$ kcal/mol) would be a much better variational choice, and suppose that this would apply to the quantum case. However, in a different quantum centroid mean-force (qcmf) approach for an asymmetric reaction such as the present one, Borgis and Azzouz (ref 18d) found that the qcmf peak shifts backward to smaller r_1 in a weakly exothermic reaction. This is precisely the direction consistent with our present TS location, for a much more exothermic reaction. This strongly suggests to us that an alternative qcmf approach would also find the present TS, but this awaits subsequent confirmation.
- (55) Another possible consequence of the quantum character of the solvent (librational) motion would be its tunneling through the barrier of the solvent free energy curves. This is not important for the first proton transfer step because the barrier is low. The effect on the second step may be considered within the harmonic bath model (e.g. ref 18a). We feel, however, that these may be considered as separate issues from the adiabatic separation approximation between the proton and the solvent coordinates.
- (56) Ebert, L. *Naturwissenschaften* **1925**, 13, 393. Robinson, R. A. *Trans. Faraday Soc.* **1936**, 32, 743.
- (57) Press, W. L.; Flannery, B. P.; Teukolsky, S. A.; Vetterling, W. T. *Numerical Recipes; The Art of Scientific Computing*; Cambridge: New York, 1989.
- (58) Conway, B. E. In *Mod. Aspects Electrochem.* Bockris, J. O'M., Conway, B. E., Eds.; Butterworths: London, 1964. Lau, Y. K.; Ikuta, S.; Kebarle, P. *J. Am. Chem. Soc.* **1982**, 104, 1462.
- (59) Robinson, G. W.; Thistlethwaite, P. J.; Lee, J. *J. Phys. Chem.* **1986**, 90, 4224.
- (60) Del Bene, J. E.; Frisch, M. J.; Luke, B. T.; Pople, J. A. *J. Phys. Chem.* **1983**, 87, 3279. Frisch, M. J.; Pople, J. A.; Del Bene, J. E. *Ibid.* **1985**, 89, 3664. Del Bene, J. E.; Frisch, M. J.; Pople, J. A. *Ibid.* **1985**, 89, 3669. Clementi, E. *Ibid.* **1985**, 89, 4426.
- (61) Similar kind of solvent motion in the second hydration shell has been suggested in a very recent *ab initio* molecular dynamics simulation work of a classical proton dynamics in 32 water molecules. Tuckerman, M. E.; Laasonen, K.; Sprik, M.; Parrinello, M. *J. Chem. Phys.* **1995**, 103, 105; *J. Phys. Chem.* **1995**, 99, 5749. For a review, see: Tuckerman, M. E.; Ungar, P. J.; von Rosenzweig, T.; Klein, M. L. *Ibid.* **1996**, 100, 12878. See also a consideration in: Agmon, N. *Chem. Phys. Lett.* **1995**, 244, 456.
- (62) Hüchel, Bernal, and Fowler and Conway *et al.* suggested that the proton transport in water is controlled by the rotation of a water molecule. The rotational motion implied or indicated there is that of the *proton-accepting water molecule* and is different from that identified here. Hüchel, E. Z. *Elektrochem.* **1928**, 34, 546. Bernal, J. D.; Fowler, R. H. *J. Chem. Phys.* **1933**, 1, 515. Conway, B. E.; Bockris, J. O'M.; Linton, H. *J. Chem. Phys.* **1956**, 24, 834.
- (63) Studies of the $\text{H}_3\text{O}^+ - \text{H}_2\text{O}$ system in pure water, with attention to the influence of the O–O distance, include in addition to refs 23 and 24: Janoschek, R.; Weidemann, E. G.; Pfeiffer, H.; Zundel, G. *J. Am. Chem. Soc.* **1972**, 94, 2387. Muñiz, A. M.; Bertrán, J.; Andrés, J. L.; Duran, M.; Lledós, A. *J. Chem. Soc., Faraday Trans. 1* **1985**, 81, 1547.
- (64) This argument would break down only when the reaction exothermicity is as large as the reorganization energy of the larger charge separation, so that the $1 \rightarrow 3$ path is almost activationless while the $1 \rightarrow 2$ step enters into the so-called “inverted” region (ref 13)—this situation corresponds to an unusually large reaction exothermicity (ref 13)—this situation corresponds to an unusually large reaction exothermicity ($\Delta G \sim -\Delta G_r(1 \rightarrow 3) = -25$ kcal/mol, i.e., $\text{pK}_a \sim -19$).
- (65) A concerted double PT was favored for a special structural arrangement of $\text{HCl}(\text{H}_2\text{O})_4$ cluster by *ab initio* density functional theory calculations: Planas, M.; Lee, C.; Novoa, J. J. *J. Phys. Chem.* **1996**, 100, 16495.
- (66) Antonchenko, V. Ya.; Davydov, A. S.; Zolotariuk, A. V. *Phys. Status Solidi (b)* **1983**, 115, 631. Davydov, A. S. *Solitons in molecular systems*; Naukovaja Dumka: Kiev, 1984. Godzik, A. *Chem. Phys. Lett.* **1990**, 171, 217. For some recent reviews, see the articles by E. S. Kryachko and V. P. Sokhan in ref 2b and J. F. Nagle in ref 2b.

(67) Kim, H. J.; Hynes, J. T. *J. Chem. Phys.* **1992**, *96*, 5088. See also ref 7 for an application to proton transfer reactions.

(68) For a discussion of these issues, see also: Gehlen, J. N.; Chandler, D.; Kim, H. J.; Hynes, J. T. *J. Phys. Chem.* **1992**, *96*, 1748. Gehlen, J. N.; Chandler, D. *J. Chem. Phys.* **1992**, *97*, 4958. Kim, H. J.; Bianco, R.; Gertner, B. J.; Hynes, J. T. *J. Phys. Chem.* **1993**, *97*, 1723.

(69) For the solvent electronic polarization effects on proton transfer potentials from an alternative viewpoint, see the path integral quantum Monte Carlo study in ref 18b.

(70) The activation free energy difference between the SC and BO limits is given by $\Delta G_{SC}^{\ddagger} - \Delta G_{BO}^{\ddagger} = 1/4 (1 - (1/\epsilon_{\infty})/((1/\epsilon_{\infty}) - (1/\epsilon_0)))$. ΔG_r^{or} , where ΔG_r^{or} is the solvent orientational reorganization energy (ref 67). We assume the reorganization energy obtained from the simulation is $\Delta G_r^{\text{sim}} = \Delta G_r^{\text{or}} + \Delta G_r^{\text{el}}$, where ΔG_r^{el} is the solvent electronic polarization part, and $\Delta G_r^{\text{el}}/\Delta G_r^{\text{sim}} = (1 - (1/\epsilon_{\infty})/(1 - (1/\epsilon_0)))$, $\Delta G_r^{\text{or}}/\Delta G_r^{\text{sim}} = ((1/\epsilon_{\infty}) - (1/\epsilon_0))/(1 - (1/\epsilon_0))$. (See ref 9 for a similar discussion, which revolves around the point that in standard intermolecular potential parameterizations, the zero-frequency and high-frequency dielectric aspects are inappropriately partitioned). By using $\epsilon_0 = 78.4$, $\epsilon_{\infty} = 1.78$, and $\Delta G_r^{\text{sim}} = 12.6$ kcal/mol, we obtain 1.4 kcal/mol as an estimate for the barrier height lowering for the first proton transfer step. As a result, the ground and the first excited proton vibrational levels are lowered by 0.66 and 0.24 kcal/mol, respectively. As discussed in text, the former will reduce the net reaction barrier. (See ref 9 for related results.)

(71) Cukier, R. I.; Morillo, M. J. *J. Chem. Phys.* **1989**, *91*, 857.

(72) Nikitin, E. E. *Theory of Elementary Atomic and Molecular Processes in Gases*; Clarendon: Oxford, 1974.

(73) For example, Onuchic, J. N.; Wolynes, P. G. *J. Phys. Chem.* **1988**, *92*, 6495 and references therein.

(74) The frequency Ω represents an equilibrium (adiabatic) fluctuation of the solvent coordinate ΔE , which is smaller than that for a pure librational oscillation of water (~ 500 – 900 cm^{-1}) being softened by coupling with the other bath coordinates. See: van der Zwan, G.; Hynes, J. T. *J. Chem. Phys.* **1983**, *78*, 4174. We used $\Omega = 400$ cm^{-1} to evaluate the parameters in Table 3. See ref 48b for an evaluation of this frequency by a molecular dynamics simulation and for an examination of the linear response assumption.

(75) Hynes, J. T. In *The Theory of Chemical Reaction Dynamics*; Baer, M., Ed.; CRC: Boca Raton, FL, 1985; Vol. 4. Truhlar, D. G.; Hase, W. L.; Hynes, J. T. *J. Phys. Chem.* **1983**, *87*, 2664. Whitnell, R. M.; Wilson, K. R. *Adv. Comput. Chem.* **1993**, *4*, 67. Hänggi, P.; Talkner, P.; Borkovec, M. *Rev. Mod. Phys.* **1990**, *62*, 250. Nitzan, A. *Adv. Chem. Phys.* **1988**, *70*, 489, Part 2. Berne, B. J.; Borkovec, M.; Straub, J. E. *J. Phys. Chem.* **1988**, *92*, 3711. Truhlar, D. G.; Garrett, B. C.; Klippenstein, S. J. *Ibid.* **1996**, *100*, 12771. Voth, G. A.; Hochstrasser, R. M. *Ibid.* **1996**, *100*, 13034.

(76) Zahr, G. E.; Preston, R. K.; Miller, W. H. *J. Chem. Phys.* **1975**, *62*, 1127. Hurwitz, Y.; Rudich, Y.; Naaman, R.; Gerber, R. B. *J. Chem. Phys.* **1993**, *98*, 2941. Wolynes, P. G.; Frauenfelder, H. *Science* **1985**, *229*, 337. Straub, J. E.; Berne, B. J. *J. Chem. Phys.* **1987**, *87*, 6111.

(77) We note that the calculated $\Delta G_{23}^{\ddagger} = 0.9$ kcal/mol is smaller than the experimental activation energy of 2.4 kcal/mol for the proton conduction in water. (Luz, Z.; Meiboom, S. *J. Am. Chem. Soc.* **1964**, *86*, 4768.) Although we suspect that the difference might be related to the close

presence of the Cl^- ion, this will have to await calculations on the proton transport in water using the same potential functions.

(78) This is a very simplified statement, since we have found a certain amount of charge delocalization in the contact ion pair state (cf. Table 1). Further, the hydration states of the contact and the solvent-separated ion pairs (**2** and **3**) differ from a complete first solvation shell situation.

(79) There are no experimental results on HCl ionization time scales for, e.g., the first step; see below.

(80) The adiabatic quantization approximation for heavy atom vibrations employed in ref 9 would need modification to account for the high frequency of the water librational modes (~ 500 – 900 cm^{-1}) compared to the Cl-O and O-O vibrations [~ 130 cm^{-1} (ref 11) and ~ 160 – 180 cm^{-1} (Okumura, M.; Yeh, L. I.; Myers, J. D.; Lee, Y. T. *J. Phys. Chem.* **1990**, *94*, 3416), respectively].

(81) See: Fonseca, T. J. *J. Chem. Phys.* **1989**, *91*, 2869 and references therein. The estimate in the present work for the **2** \rightarrow **3** solvent barrier is on the very edge for the existence of a well-defined rate constant. The considerations of section VI suggest that the solvent coordinate barrier is even lower and nonexponential kinetics seem likely.

(82) We thank Professor A. Zewail for a discussion of a possibly similar situation in an excited electronic state organic acid proton transfer.

(83) It should be noticed however that an experimentally prepared larger $\text{HCl}(\text{H}_2\text{O})_n$ cluster may not have the favorable sequencing and geometry of the cluster examined in section II.B.

(84) This basic conclusion is also reached via quite different techniques in: Laasonen, K.; Klein, M. L. *J. Am. Chem. Soc.* **1994**, *116*, 11620.

(85) See, e.g., the articles in: *Ultrafast Dynamics of Chemical Systems*; Simon, J. D., Ed.; Kluwer Academic Publishers: Dordrecht, 1994. *Ultrafast Reaction Dynamics and Solvent Effects*; Gauduel, Y., Rossky, P. J., Eds.; AIP Press: New York, 1994. For a recent review on solvation dynamics, see e.g.: Stratt, R. M.; Maroncelli, M. *J. Phys. Chem.* **1996**, *100*, 12981.

(86) A simulation study on the acidity of HCl relative to water in ambient and supercritical water is recently performed in: Balbuena, P. B.; Johnston, K. P.; Rossky, P. J. *J. Phys. Chem.* **1996**, *100*, 2716.

(87) Heger, K.; Uematsu, M.; Franck, E. U. *Ber. Bunsen-Ges. Phys. Chem.* **1980**, *84*, 758. Marshall, W. L.; Franck, E. U. *J. Phys. Chem. Ref. Data* **1980**, *10*, 295.

(88) For a related phenomenon for NaCl ionization, see: Gao, J. *J. Phys. Chem.* **1994**, *98*, 6049. Cui, S. T.; Harris, J. G. *Chem. Eng. Sci.*, in press.

(89) Staib, A.; Hynes, J. T. Work in progress. Ando, K.; Staib, A.; Hynes, J. T. In *Femtochemistry: Ultrafast Chemical and Physical Processes in Molecular Systems*; Chergui, M., Ed.; World Scientific: Singapore, 1996.

(90) Gertner, B. J.; Hynes, J. T. *Science* **1996**, *271*, 1563.

(91) Hanson, D. R.; Ravishankara, A. R. *J. Phys. Chem.* **1992**, *96*, 2682. Kroes, G.-J.; Clary, D. C. *J. Phys. Chem.* **1992**, *96*, 7079. Graham, J. D.; Roberts, J. T. *J. Phys. Chem.* **1994**, *98*, 5974.

(92) Mulliken, R. S. *J. Phys. Chem.* **1952**, *56*, 801; *J. Chim. Phys.* **1964**, *20*, 20. Coulson, C. A. In *Hydrogen Bonding*; Hadži, D., Thompson, H. W., Eds.; Pergamon: London, 1959. Bratož, S. *Adv. Quantum Chem.* **1967**, *3*, 209. Ilczyszyn, M.; Ratajczak, H.; Skowronek, K. *Magn. Reson. Chem.* **1988**, *26*, 445. Ratajczak, H.; Orville-Thomas, W. J.; Rao, C. N. R. *Chem. Phys.* **1976**, *17*, 197. Hasegawa, M.; Daiyasu, K.; Yomosa, S. *J. Phys. Soc. Jpn.* **1970**, *28*, 275, 1304. Reed, A. E.; Curtis, L. A.; Weinhold, F. *Chem. Rev.* **1988**, *88*, 899.